RSC Advances

PAPER

View Article Online
View Journal | View Issue

Cite this: *RSC Adv.*, 2026, **16**, 17085

Multitarget synthetic piperates against key drug targets of Alzheimer's and diabetes mellitus

Asif Ahmad,[a] Uzma Salar, *[b] Musa Özil, [c] Nimet Baltaş,[c] Maria Nasim,[b] Aaqib Ullah,[a] Zaheer Ul-Haq,[b] Khalid Mohammed Khan[de] and Farzana Shaheen*[a]

A library of piperate derivatives **3–25** was synthesized in a two-step reaction scheme starting from piperine **1**, which was converted to piperic acid **2** first, and then reacted with various alkyl and aryl halides to afford the final products. Compounds were fully characterized and evaluated for their multitarget potential against well-established drug targets involved in diabetes and Alzheimer's diseases. *In vitro* assay revealed strong inhibitory activity against acetylcholinesterase (AChE), butylcholinesterase (BChE), α-glucosidase, and α-amylase. Compounds **6–15**, **19**, and **21–23** were potent inhibitors of AChE, and compounds **6–8**, **12–15**, **19**, and **21–23** were also more effective inhibitors of BChE than the standard donepezil. Compounds bearing halogens (F, Cl, and Br) exhibited noteworthy inhibitory potency against both targets. In addition, compounds **2**, **3**, **17**, **18**, and **25** were recognized as potent α-glucosidase and α-amylase inhibitors, outperforming standard acarbose. In particular, piperic acid (2) and compounds containing the cyanomethyl (compound **3**), 3-methoxyphenyl (compounds **17**, **18**), and 2-nitrophenyl (compound **25**) moieties showed remarkable inhibitory potential. Further, kinetic studies were conducted to unravel the inhibition mechanism against all four enzymes, while *in silico* studies identified key interactions between inhibitors and the active-site residues of each target. All compounds also displayed reasonable antioxidant potential, as evidenced by FRAP, CUPRAC, and DPPH assays, compared with the standard butylated hydroxytoluene (BHT). Detailed pharmacokinetic and ADME profiles were also predicted to assess the druggability of the compounds. The identified ligands have multitarget potential to inhibit the key enzymes associated with diabetes and Alzheimer's. They may serve as lead candidates for later stages of drug development.

Received 31st January 2026
Accepted 20th March 2026

DOI: 10.1039/d6ra00843g

rsc.li/rsc-advances

Introduction

Alzheimer's disease (AD), the most prevalent type of dementia, is a progressive neurodegenerative disorder characterized by gradual cognitive deterioration, memory impairment, and behavioral disturbances. It affects over 55 million people worldwide, standing as the seventh leading cause of death altogether.[1] Its prevalence is projected to rise to 78 million by 2030 and 139 million by 2050, posing a significant public health concern. Although its precise underlying cause remains unclear, key pathological mechanisms include tau protein aggregation, cholinergic dysfunction,[2] extracellular amyloid-β (Aβ) deposition,[3] and increased disruption of redox homeostasis.[4,5] Advanced glycation end-products (AGEs), generated through the non-enzymatic Maillard reaction between reducing sugars and proteins, are key contributors to the development of AD. Glycation of tau and Aβ peptides in the AD brain promotes the growth of senile plaques and neurofibrillary tangles. AGEs also interact with the RAGE (receptor for advanced glycation end-products), generating ROS (reactive oxygen species) and triggering vascular inflammation. The AGE-RAGE interaction alters gene expression and exacerbates AD pathology. Oxidative stress further contributes to the disease by damaging lipids, proteins, and DNA, reinforcing the "oxidative stress" hypothesis, which positions ROS as central to AD onset and progression. Therapeutic strategies that inhibit ROS or reduce their formation are considered promising.[6–8]

Cholinergic dysfunction, primarily due to reduced acetylcholine (ACh) levels and elevated acetylcholinesterase (AChE) activity, also contributes to AD-related cognitive decline. The cholinergic hypothesis attributes these symptoms to the degeneration of cholinergic neurons and rapid ACh breakdown.

[a]*Third World Center for Science and Technology, H. E. J. Research Institute of Chemistry, International Center for Chemical and Biological Sciences, University of Karachi, Karachi 75270, Pakistan. E-mail: farzana.shaheen@iccs.edu; Tel: +92-21111222292 ext. 136*

[b]*Dr Panjwani Center for Molecular Medicine and Drug Research, International Center for Chemical and Biological Sciences, University of Karachi, Karachi-75270, Pakistan. E-mail: uzma_salar_sheikh@hotmail.com; uzma.salar@iccs.edu*

[c]*Department of Chemistry, Recep Tayyip Erdogan University, 53100 Rize, Turkey*

[d]*H. E. J. Research Institute of Chemistry, International Center for Chemical and Biological Sciences, University of Karachi, Karachi 75270, Pakistan*

[e]*Department of Clinical Pharmacy, Institute for Research and Medical Consultations (IRMC), Imam Abdulrahman Bin Faisal University, P.O. Box 31441, Dammam, Saudi Arabia*

AChE and butyrylcholinesterase (BChE) inhibitors can enhance synaptic ACh and improve cognition.[9,10] However, current treatments are mainly limited to AChE inhibitors and offer only symptomatic relief. Given AD's multifactorial nature, multi-target-directed ligands and combination therapies are being explored for more effective interventions.[11–13]

Diabetes mellitus (DM) is a lasting metabolic disorder, currently affecting over 400 million individuals worldwide. It disrupts carbohydrate, protein, and fat metabolism due to insufficient insulin or hormonal imbalance. Over the past two decades, diabetes prevalence has surged, making it a major 21st-century public health challenge. According to the International Diabetes Federation (IDF, 2021), the number of adults living with diabetes has tripled, reaching 537 million, and is projected to increase to 643 million by 2030 and 783 million by 2045.[14] Diabetes mellitus (DM) is classified into Type 1 (T1DM), which results from autoimmune-mediated destruction of pancreatic β-cells, and Type 2 (T2DM), characterized by insulin resistance and/or impaired insulin secretion.[15] Both forms lead to chronic hyperglycemia, which promotes protein glycation and the subsequent formation of advanced glycation end products (AGEs).

AGEs contribute significantly to macrovascular and microvascular complications.[16] Early diagnosis and targeted therapies are essential to reduce the disease burden and prevent long-term complications. An effective strategy for managing diabetes and its complications involves regulating postprandial blood glucose by inhibiting carbohydrate-digesting enzymes. α-Glucosidase and α-amylase, located in the small intestine's brush border, are key glycoside hydrolases in this process. α-Amylase breaks down polysaccharides into oligosaccharides and disaccharides, while α-glucosidase cleaves α-glucopyranoside bonds to release glucose.[17] Inhibiting these enzymes slows glucose absorption, thereby reducing postprandial hyperglycemia. As a result, glycoside hydrolase inhibitors have gained attention as promising therapeutic agents for diabetes and related metabolic disorders.[18]

Reactive oxygen species (ROS), produced during normal metabolism, play roles in cellular signaling at low concentrations. However, when ROS overwhelm the body's antioxidant defenses, oxidative stress occurs. It leads to damage of proteins, DNA, lipids, and other macromolecules, disrupting cellular homeostasis. Oxidative stress plays a crucial role in the development of numerous diseases, such as Alzheimer's disease, diabetes, cancer, myocardial infarction, atherosclerosis, autoimmune conditions, and chronic inflammatory disorders.[19,20]

The complex, multifactorial nature of AD and DM demands polyfunctional agents capable of modulating multiple pathways simultaneously. Such compounds offer advantages over single-target drugs by combining diverse biological activities with a unified pharmacokinetic profile.[21] This study explores polyfunctional molecules derived from piperine, the principal alkaloid of black pepper, targeting cholinesterases, hydrolases, and oxidative stress for the effective treatment of AD and DM. Piperine and its derivatives are well known for their diverse pharmacological properties, including antidiabetic, antioxidant, antimicrobial, and neuroprotective effects, as well as activity against cognitive impairment in AD.[22–26] Our research group has previously reported piperine-based scaffolds with analgesic and antiinflammatory activities under the framework of Biology-Oriented Synthesis (BIOS).[27] In continuation of this work, and considering the growing therapeutic relevance of piperine, we designed and evaluated a series of piperine derivatives against key enzymes associated with AD and DM.

Experimental

Materials and methods

All chemicals/reagents were purchased from Sigma-Aldrich, USA. Thin-layer chromatography was performed on pre-coated silica gel, GF-254 (Merck, Germany). Spots were visualized under ultraviolet light at 254 and 366 nM. MAT 312 and MAT 113D mass spectrometers were used for the EI-MS and HR-EIMS analysis of compounds. The ^{1}H-NMR was recorded on Bruker Avance Neo spectrometers, operating at 400 MHz, while the ^{13}C-NMR was recorded at 100 MHz. The chemical shift values are presented in ppm (δ), and the coupling constant (J) is in Hz. Melting points of the compounds were determined on a Stuart® SMP10 melting point apparatus and are uncorrected.

General protocol for synthesis of piperic acid (2). 20 mmol of piperine was dissolved in 100 mL of ethanol. 10 g potassium hydroxide was introduced, and the reaction mixture was refluxed overnight. TLC (EtOAc : Hex 3 : 7) was examined to monitor the reaction progress. After completion, the reaction was allowed to cool. On cooling, precipitates formed, which were filtered and washed with excess water to obtain a pure product. The product was crystallized from ethanol.

(2*E*,4*E*)-5-(benzo[*d*][1,3]dioxol-5-yl)penta-2,4-dienoic acid (2). Brown Color; 78% yield; M.P. 280–292 °C; EI-MS *m*/*z* (% rel. abund.): 218 (M^+, 80), 173 (95), 143 (47), 115 (100); HREI-MS *m*/*z*: calcd for $C_{12}H_{10}O_4$ [218.0579], found [218.0587]; ^{1}H-NMR (500 MHz, DMSO-d_6): δ_H 7.20 (s, 1H, H-4), 7.18 (dd, $J_{12,11} = J_{12,13} =$ 14.9 Hz, 1H, H-12), 6.98 (d, $J_{6,7} = 8.0$ Hz, 1H, H-6), 6.92 (ovp, 3H, H-7, H-10, H-11), 6.03 (s, 2H, CH_2-2), 5.91 (d, $J_{13,12} = 15.1$ Hz, 1H, H-13); IR (KBr, cm^{-1}): 2910 (C–H), 1695 (C=O), 1449 (C=C).

General protocol for syntheses of alkyl and aryl piperate derivatives (3–25). One mmol of piperic acid was taken in 10 mL acetonitrile, and then 1 mmol of alkyl or aryl halide and 1 mmol of trimethylamine were added to it. Reaction refluxed with stirring overnight. TLC (EtOAc : Hex 3 : 7) was examined to monitor the reaction progress. After completion, the reaction was allowed to cool, resulting in precipitate formation, which was filtered and then extensively washed with water to produce a pure product. The product was crystallized from acetonitrile. As per the literature, apart from piperic acid **2**,[25] structures of compounds **4** and **20** (ref. 28 and 29) are previously known.

Cyanomethyl (2*E*,4*E*)-5-(benzo[*d*][1,3]dioxol-5-yl)penta-2,4-dienoate (3). Light yellow color; 81% yield; M.P. 214–216 °C; EI-MS *m*/*z* (% rel. abund.): 257 (M^+, 64), 217 (7), 201 (26), 173 (87), 143 (54), 115 (100); HREI-MS *m*/*z*: calcd for $C_{14}H_{11}O_4N$ [257.0688], found [257.0699]; ^{1}H-NMR (400 MHz, DMSO-d_6): δ_H 7.51 (dd, $J_{12,11} = J_{12,13} = 14.4$ Hz, 1H, H-12), 7.24 (d, $J_{4,6} = 1.0$ Hz, 1H, H-4), 7.12 (ovp, 3H, H-6, H-10, H-11), 6.94 (d, $J_{7,6} = 8.0$ Hz,

1H, H-7), 6.07 (d, $J_{13,12}$ = 16.0 Hz, 1H, H-13), 6.05 (s, 2H, CH_2-2), 6.03 (s, 2H, CH_2-16); IR (KBr, cm^{-1}): 1688 (C=O), 1448 (C=C).

Pentyl (2*E*,4*E*)-5-(benzo[*d*][1,3]dioxol-5-yl)penta-2,4-dienoate (4). Light brown color; 79% yield; M.P. 315–317 °C; EI-MS *m*/*z* (% rel. abund.): 288 (M^+, 65), 217 (11), 201 (35), 187 (4), 173 (100), 143 (55); HREI-MS *m*/*z*: calcd for $C_{17}H_{20}O_4$ [288.1362], found [288.1358]; ^{1}H-NMR (400 MHz, DMSO-d_6): δ_H 7.36 (dd, $J_{12,11} = J_{12,13}$ = 15.2 Hz, 1H, H-12), 7.20 (d, $J_{4,6}$ = 1.0 Hz, 1H, H-4), 7.02 (ovp, 3H, H-6, H-10, H-11), 6.91 (d, $J_{7,6}$ = 8.0 Hz, 1H, H-7), 6.03 (s, 2H, CH_2-2), 5.99 (d, $J_{13,12}$ = 15.2 Hz, 1H, H-13), 4.08 (t, $J_{16,17}$ = 6.6 Hz, 2H, CH_2-16), 1.60 (q, 2H, CH_2-17), 1.30 (ovp, 4H, CH_2-18, CH_2-19), 0.87 (t, $J_{20,19}$ = 6.8 Hz, 3H, CH_3-20); IR (KBr, cm^{-1}): 1698 (C=O), 1447 (C=C).

But-3-en-1-yl (2*E*,4*E*)-5-(benzo[*d*][1,3]dioxol-5-yl)penta-2,4-dienoate (5). Brown color; 78% yield; M.P. 149–151 °C; EI-MS *m*/*z* (% rel. abund.): 272 (M^+, 100), 218 (12), 201 (37), 187 (2), 173 (75); HREI-MS *m*/*z*: calcd for $C_{16}H_{16}O_4$ [272.1049], found [272.1042]; ^{1}H-NMR (400 MHz, DMSO-d_6): δ_H 7.36 (dd, $J_{12,11} = J_{12,13}$ = 15.2 Hz, 1H, H-12), 7.20 (d, $J_{4,6}$ = 1.0 Hz, 1H, H-4), 7.00 (ovp, 3H, H-6, H-7, H-10, H-11), 6.03 (s, 2H, CH_2-2), 5.98 (d, $J_{13,12}$ = 15.2 Hz, 1H, H-13), 5.84 (m, 1H, H-18), 5.12 (dd, $J_{19,18}$ = 17.2 Hz, 2H, CH_2-19), 4.14 (t, $J_{16,17}$ = 6.5 Hz, 2H, CH_2-16), 2.38 (m, 2H, CH_2-17); IR (KBr, cm^{-1}): 2908 (C–H), 1698 (C=O), 1621, 1446 (C=C).

4-Bromobenzyl (2*E*,4*E*)-5-(benzo[*d*][1,3]dioxol-5-yl)penta-2,4-dienoate (6). Brown color; 79% yield; M.P. 221–223 °C; EI-MS *m*/*z* (% rel. abund.): 386 (M^+, 14), 388 (M + 2, 13), 217 (100), 171 (49), 115 (49); HREI-MS *m*/*z*: calcd for $C_{19}H_{15}BrO_4$ [386.0154], found [386.0147]; ^{1}H-NMR (400 MHz, DMSO-d_6): δ_H 7.58 (d, $J_{2',3'} = J_{6',5'}$ = 8.36 Hz, 1H, H-2′, H-6′), 7.36 (ovp, 3H, H-12, H-3′, H-5′), 7.22 (s, 1H, H-4), 7.01 (ovp, 3H, H-6, H-10, H-11), 6.93 (d, $J_{7,6}$ = 8.04 Hz, 1H, H-7), 6.05 (d, $J_{13,12}$ = 16.0 Hz, 1H, H-13), 6.04 (s, 2H, CH_2-2), 5.14 (s, 2H, CH_2-16); IR (KBr, cm^{-1}): 1698 (C=O), 1448 (C=C), 669 (C–Br).

2-Bromobenzyl (2*E*,4*E*)-5-(benzo[*d*][1,3]dioxol-5-yl)penta-2,4-dienoate (7). Brown color; 71% yield; M.P. 98–100 °C; EI-MS *m*/*z* (% rel. abund.): 386 (M^+, 41), 388 (M + 2, 41), 305 (4), 217 (100), 201 (15), 187 (21), 173 (42); HREI-MS *m*/*z*: calcd for $C_{19}H_{15}O_4Br$ [386.0154], found [386.0143]; ^{1}H-NMR (400 MHz, DMSO-d_6): δ_H 7.67 (d, $J_{3',4'}$ = 7.3 Hz, 1H, H-3′), 7.52 (d, $J_{6',5'}$ = 7.6 Hz, $J_{6',4'}$ = 1.3 Hz, 1H, H-6′), 7.45 (m, 2H, H-5′, H-12), 7.32 (dt, $J_{4'(3',5')}$ = 7.6 Hz, $J_{4',6'}$ = 1.3 Hz, 1H, H-4′), 7.22 (d, $J_{4,6}$ = 1.2 Hz, 1H, H-4), 7.07 (ovp, 3H, H-6, H-10, H-11), 6.93 (d, $J_{7,6}$ = 8.0 Hz, 1H, H-7), 6.08 (d, $J_{13,12}$ = 14.2 Hz, 1H, H-13), 6.04 (s, 2H, CH_2-2), 5.20 (s, 2H, CH_2-16); IR (KBr, cm^{-1}): 1697 (C=O), 1448 (C=C), 724 (C–Br).

4-Chlorobenzyl (2*E*,4*E*)-5-(benzo[*d*][1,3]dioxol-5-yl)penta-2,4-dienoate (8). Grey color; 88% yield; M.P. 101–103 °C; EI-MS *m*/*z* (% rel. abund.): 342 (M^+, 43), 344 (M + 2, 16), 259 (7), 217 (100), 201 (8), 187 (19), 173 (16); HREI-MS *m*/*z*: calcd for $C_{19}H_{15}O_4Cl$ [342.0659], found [342.0668]; ^{1}H-NMR (400 MHz, DMSO-d_6): δ_H 7.45 (ovp, 5H, H-2′, H-3′, H-5′, H-6′, H-12), 7.21 (d, $J_{4,6}$ = 1.0 Hz, 1H, H-4), 7.06 (ovp, 3H, H-6, H-10, H-11), 6.95 (d, $J_{7,6}$ = 8.0 Hz, 1H, H-7), 6.05 (d, $J_{13,12}$ = 15.2 Hz, 1H, H-13), 6.04 (s, 2H, CH_2-2), 5.15 (s, 2H, CH_2-16); IR (KBr, cm^{-1}): 1698 (C=O), 1447 (C=C), 710 (C–Cl).

3,4-Dichlorobenzyl (2*E*,4*E*)-5-(benzo[*d*][1,3]dioxol-5-yl)penta-2,4-dienoate (9). Brown color; 86% yield; M.P. 118–120 °C; EI-MS *m*/*z* (% rel. abund.): 376 (M^+, 56), 378 (M + 2, 38), 380 (M + 4, 7), 217 (100), 201 (11), 187 (25), 173 (47), 159 (48); HREI-MS *m*/*z*: calcd for $C_{19}H_{14}O_4Cl_2$ [376.0269], found [376.0257]; ^{1}H-NMR (400 MHz, DMSO-d_6): δ_H 7.67 (d, $J_{2',6'}$ = 1.7 Hz, 1H, H-2′), 7.65 (d, $J_{5',6'}$ = 8.2 Hz, 1H, H-5′), 7.45 (ovp, 2H, H-6′, H-12), 7.22 (d, $J_{4,6}$ = 1.0 Hz, 1H, H-4), 7.06 (ovp, 3H, H-6, H-10, H-11), 6.93 (d, $J_{7,6}$ = 8.0 Hz, 1H, H-7), 6.07 (d, $J_{13,12}$ = 15.2 Hz, 1H, H-13), 6.04 (s, 2H, CH_2-2), 5.16 (s, 2H, CH_2-16); IR (KBr, cm^{-1}): 1698 (C=O), 1445 (C=C), 722 (C–Cl).

2,4-Dichlorobenzyl (2*E*,4*E*)-5-(benzo[*d*][1,3]dioxol-5-yl)penta-2,4-dienoate (10). Brown color; 69% yield; M.P. 112–114 °C; EI-MS *m*/*z* (% rel. abund.): 376 (M^+, 41), 378 (M + 2, 27), 380 (M + 4, 5), 217 (100), 201 (17), 187 (36), 173 (46), 159 (81); HREI-MS *m*/*z*: calcd for $C_{19}H_{14}Cl_2O_4$ [376.0269], found [376.0273]; ^{1}H-NMR (400 MHz, DMSO-d_6): δ_H 7.67 (d, $J_{3',5'}$ = 2.0 Hz, 1H, H-3′), 7.55 (d, $J_{6',5'}$ = 8.3 Hz, 1H, H-6′), 7.48 (dd, $J_{5',6'}$ = 8.3 Hz, $J_{5',3'}$ = 2.0 Hz, 1H, H-5′), 7.42 (d, $J_{12,11} = J_{12,13}$ = 15.2 Hz, 1H, H-12), 7.22 (d, $J_{4,6}$ = 1.0 Hz, 1H, H-4), 7.06 (ovp, 3H, H-6, H-10, H-11), 6.93 (d, $J_{7,6}$ = 8.0 Hz, 1H, H-7), 6.07 (d, $J_{13,12}$ = 15.2 Hz, 1H, H-13), 6.03 (s, 2H, CH_2-2), 5.21 (s, 2H, CH_2-16); IR (KBr, cm^{-1}): 1698 (C=O), 1445 (C=C), 755 (C–Cl).

2,6-Dichlorobenzyl (2*E*,4*E*)-5-(benzo[*d*][1,3]dioxol-5-yl)penta-2,4-dienoate (11). Yellow color; 77% yield; M.P. 128–130 °C; EI-MS *m*/*z* (% rel. abund.): 376 (M^+, 59), 378 (M + 2, 38), 380 (M + 4, 7), 217 (100), 201 (20), 187 (28), 173 (71); HREI-MS *m*/*z*: calcd for $C_{19}H_{14}Cl_2O_4$ [376.0269], found [376.0276]; ^{1}H-NMR (400 MHz, DMSO-d_6): δ_H 7.55 (d, $J_{3',4'} = J_{5',4'}$ = 8.1 Hz, 1H, H-3′, H-5′), 7.47 (m, 1H, H-4′), 7.40 (dd, $J_{12,11} = J_{12,13}$ = 15.2 Hz, 1H, H-12), 7.20 (d, $J_{4,6}$ = 1.0 Hz, 1H, H-4), 7.05 (ovp, 3H, H-6, H-10, H-11), 6.92 (d, $J_{7,6}$ = 8.0 Hz, 1H, H-7), 6.03 (s, 2H, CH_2-2), 6.01 (d, $J_{13,12}$ = 15.2 Hz, 1H, H-13), 5.35 (s, 2H, CH_2-16); IR (KBr, cm^{-1}): 1698 (C=O), 1445 (C=C), 723 (C–Cl).

2-Chloro-4-fluorobenzyl (2*E*,4*E*)-5-(benzo[*d*][1,3]dioxol-5-yl) penta-2,4-dienoate (12). White color; 83% yield; M.P. 110–111 °C; EI-MS *m*/*z* (% rel. abund.): 360 (M^+, 49), 362 (M + 2, 18), 217 (100), 201 (19), 187 (33), 173 (40), 143 (98), 115 (65); HREI-MS *m*/*z*: calcd for $C_{19}H_{14}O_4ClF$ [360.0565], found [360.0565]; ^{1}H-NMR (400 MHz, DMSO-d_6): δ_H 7.61 (dd, $J_{3',F'} = J_{3',Cl}$ = 8.52 Hz, 1H, H-3′), 7.52 (dd, $J_{6',5'}$ = 8.7 Hz, $J_{6',F}$ = 2.6 Hz, 1H, H-6′), 7.44 (dd, $J_{12,11} = J_{12,13}$ = 15.0 Hz, 1H, H-12), 7.28 (dt, $J_{5'(6',F)}$ = 8.5 Hz, $J_{5',3'}$ = 2.5 Hz, 1H, H-5′), 7.22 (s, 1H, H-4), 7.02 (ovp, 3H, H-6, H-10, H-11), 6.93 (d, $J_{7,6}$ = 8.0 Hz, 1H, H-7), 6.05 (d, $J_{13,12}$ = 15.1 Hz, 1H, H-13), 6.04 (s, 2H, CH_2-2), 5.21 (s, 2H, CH_2-16); ^{13}C-NMR (100 MHz DMSO-d_6): δ 165.80, 162.75, 160.77, 148.29, 147.97, 145.89, 141.02, 133.84, 132.20, 130.32, 124.53, 123.34, 119.01, 116.91, 114.59, 108.52, 105.71, 101.39, 62.34; IR (KBr, cm^{-1}): 1700 (C=O), 1446 (C=C), 1233 (C–F), 754 (C–Cl).

2-Fluorobenzyl (2*E*,4*E*)-5-(benzo[*d*][1,3]dioxol-5-yl)penta-2,4-dienoate (13). Light brown color; 73% yield; M.P. 163–165 °C; EI-MS *m*/*z* (% rel. abund.): 326 (M^+, 80), 285 (9), 243 (8), 217 (100), 201 (30), 187 (34), 109 (84.2); HREI-MS *m*/*z*: calcd for $C_{19}H_{15}FO_4$ [326.0954], found [326.0962]; ^{1}H-NMR (400 MHz, DMSO-d_6): δ_H 7.50 (t, $J_{3',4'} = J_{3',F}$ = 7.6 Hz, 1H, H-3′), 7.44 (ovp, 2H, H-5′, H-12), 7.25 (ovp, 3H, H-4, H-4′, H-6′), 7.02 (ovp, 3H, H-

6, H-10, H-11), 6.92 (d, $J_{7,6}$ = 8.0 Hz, 1H, H-7), 6.04 (d, $J_{13,12}$ = 13.6 Hz, 1H, H-13), 6.04 (s, 2H, CH_2-2), 5.21 (s, 2H, CH_2-16); ^{13}C-NMR (100 MHz DMSO-d_6): δ 165.85, 148.27, 147.97, 145.78, 140.95, 130.87, 130.57, 130.51, 130.34, 124.53, 124.49, 123.32, 119.12, 115.45, 115.28, 108.52, 105.70, 101.38, 59.55; IR (KBr, cm^{-1}): 1699 (C=O), 1445 (C=C), 1233 (C–F).

4-(Trifluoromethyl)benzyl (2*E*,4*E*)-5-(benzo[*d*][1,3]dioxol-5-yl)penta-2,4-dienoate (14). Yellow color; 65% yield; M.P. 122–124 °C; EI-MS *m*/*z* (% rel. abund.): 376 (M^+, 100), 357 (11), 217 (54), 201 (18), 187 (22), 173 (92); HREI-MS *m*/*z*: calcd for $C_{20}H_{15}O_4F_3$ [376.0922], found [376.0910]; ^{1}H-NMR (400 MHz, DMSO-d_6): δ_H 7.75 (d, $J_{3',2'} = J_{5',6'}$ = 8.1 Hz, 1H, H-3′, H-5′), 7.61 (d, $J_{2',3'} = J_{6',5'}$ = 8.3 Hz, 2H, H-2′, H-6′), 7.46 (ddd, $J_{12,11} = J_{12,13}$ = 15.2 Hz, 1H, H-12), 7.22 (d, $J_{4,6}$ = 1.0 Hz, 1H, H-4), 7.07 (ovp, 3H, H-6, H-10, H-11), 6.93 (d, $J_{7,6}$ = 8.0 Hz, 1H, H-7), 6.08 (d, $J_{13,12}$ = 15.2 Hz, 1H, H-13), 6.04 (s, 2H, CH_2-2), 5.27 (s, 2H, CH_2-16); IR (KBr, cm^{-1}): 1698 (C=O), 1445 (C=C), 1251 (C–F).

3-(Trifluoromethyl)benzyl (2*E*,4*E*)-5-(benzo[*d*][1,3]dioxol-5-yl)penta-2,4-dienoate (15). Grey color; 87% yield; M.P. 241–243 °C; EI-MS *m*/*z* (% rel. abund.): 376 (M^+, 100), 357 (9), 217 (58), 201 (19), 187 (25), 173 (91), 159 (65); HREI-MS *m*/*z*: calcd for $C_{20}H_{15}O_4F_3$ [376.0922], found [376.0931]; ^{1}H-NMR (400 MHz, DMSO-d_6): δ_H 7.75 (ovp, 3H, H-2′, H-4′, H-6′), 7.64 (t, $J_{5'(4',6')}$ = 7.6 Hz, 1H, H-5′), 7.45 (dd, $J_{12,11} = J_{12,13}$ = 15.2 Hz, 1H, H-12), 7.22 (d, $J_{4,6}$ = 0.8 Hz, 1H, H-4), 7.06 (ovp, 3H, H-6, H-10, H-11), 6.93 (d, $J_{7,6}$ = 8.0 Hz, 1H, H-7), 6.08 (d, $J_{13,12}$ = 15.2 Hz, 1H, H-13), 6.04 (s, 2H, CH_2-2), 5.26 (s, 2H, CH_2-16); IR (KBr, cm^{-1}): 1698 (C=O), 1446 (C=C), 1061 (C–F).

4-Isopropylbenzyl (2*E*,4*E*)-5-(benzo[*d*][1,3]dioxol-5-yl)penta-2,4-dienoate (16). Brown color; 84% yield; M.P. 91–93 °C; EI-MS *m*/*z* (% rel. abund.): 350 (M^+, 66), 267 (74), 217 (84), 201 (14), 187 (18), 173 (18), 133 (100); HREI-MS *m*/*z*: calcd for $C_{22}H_{22}O_4$ [350.1518], found [350.1520]; ^{1}H-NMR (400 MHz, DMSO-d_6): δ_H 7.42 (dd, $J_{12,11} = J_{12,13}$ = 15.2 Hz, 1H, H-12), 7.31 (d, $J_{3',2'} = J_{5',6'}$ = 8.0 Hz, 1H, H-3′, H-5′), 7.25 (d, $J_{2',3'} = J_{6',5'}$ = 8.0 Hz, 2H, H-2′, H-6′), 7.21 (s, 1H, H-4), 7.07 (ovp, 3H, H-6, H-10, H-11), 6.92 (d, $J_{7,6}$ = 8.0 Hz, 1H, H-7), 6.04 (d, $J_{13,12}$ = 15.4 Hz, 1H, H-13), 6.04 (s, 2H, CH_2-2), 5.11 (s, 2H, CH_2-16), 2.92 (sept, 1H, H-7′), 1.19 (d, $J_{8',7'} = J_{9',7'}$ = 7.0 Hz, 1H, CH_3-8′, CH_3-9′); IR (KBr, cm^{-1}): 2912 (C–H), 1698 (C=O), 1445 (C=C).

3-Methoxybenzyl (2*E*,4*E*)-5-(benzo[*d*][1,3]dioxol-5-yl)penta-2,4-dienoate (17). Yellow color; 77% yield; M.P. 112–114 °C; EI-MS *m*/*z* (% rel. abund.): 338 (M^+, 76), 255 (27), 217 (100), 201 (16), 187 (18), 173 (17), 121 (69); HREI-MS *m*/*z*: calcd for $C_{20}H_{18}O_5$ [338.1154], found [338.1148]; ^{1}H-NMR (400 MHz, DMSO-d_6): δ_H 7.39 (dd, $J_{12,11} = J_{12,13}$ = 15.2 Hz, 1H, H-12), 7.30 (d, $J_{5'(4',6')}$ = 8.0 Hz, 1H, H-5′), 7.21 (d, $J_{2',4'}$ = 1.0 Hz, 1H, H-2′), 7.05 (ovp, 7H, H-4′, H-6′, H-4, H-6, H-7, H-10, H-11), 6.05 (d, $J_{13,12}$ = 15.2 Hz, 1H, H-13), 6.03 (s, 2H, CH_2-2), 5.12 (s, 2H, CH_2-16), 3.73 (s, 3H, OCH_3); IR (KBr, cm^{-1}): 1698 (C=O), 1444 (C=C), 1034 (C–O).

2-(3-Methoxyphenyl)-2-oxoethyl (2*E*,4*E*)-5-(benzo[*d*][1,3]dioxol-5-yl)penta-2,4-dienoate (18). White color; 75% yield; M.P. 125–127 °C; EI-MS *m*/*z* (% rel. abund.): 366 (M^+, 2), 300 (4), 285 (76), 201 (100), 173 (33), 150 (49), 143 (27), 115 (77); HREI-MS *m*/*z*: calcd for $C_{21}H_{18}O_6$ [366.1103], found [366.1093]; ^{1}H-NMR (400 MHz, DMSO-d_6): δ_H 7.57 (dd, $J_{6',5'}$ = 7.7 Hz, 1H, H-6′), 7.49 (ovp, 3H, H-4′, H-5′, H-12), 7.27 (dd, $J_{2',4'}$ = 2.0 Hz, 1H, H-2′), 7.24 (s, 1H, H-4), 7.06 (ovp, 3H, H-6, H-10, H-11), 6.94 (d, $J_{7,6}$ = 8.0 Hz, 1H, H-7), 6.15 (d, $J_{13,12}$ = 15.0 Hz, 1H, H-13), 6.05 (s, 2H, CH_2-2), 5.54 (s, 2H, CH_2-16), 3.82 (s, 3H, OCH_3); ^{13}C-NMR (100 MHz DMSO-d_6): δ 192.74, 165.61, 159.47, 148.32, 146.07, 141.73, 141.05, 137.58, 135.26, 130.11, 125.66, 124.62, 123.39, 119.93, 118.92, 112.27, 108.54, 105.74, 101.40, 66.46, 55.40; IR (KBr, cm^{-1}): 1699 (C=O), 1446 (C=C), 1036 (C–O).

2-(5-Fluoro-2-methoxyphenyl)-2-oxoethyl (2*E*,4*E*)-5-(benzo[*d*][1,3]dioxol-5-yl)penta-2,4-dienoate (19). Yellow color; 76% yield; M.P. 134–136 °C; EI-MS *m*/*z* (% rel. abund.): 384 (M^+, 40), 201 (72), 172 (53), 153 (100); HREI-MS *m*/*z*: calcd for $C_{21}H_{17}O_6F$ [384.1009], found [384.1007]; ^{1}H-NMR (400 MHz, DMSO-d_6): δ_H 7.52 (ovp, 3H, H-4′, H-6′, H-12), 7.28(dd, $J_{3',4'}$ = 9.0 Hz, $J_{3',F}$ = 4.1 Hz, 1H, H-3′), 7.26 (s, 1H, H-4), 7.04 (ovp, 3H, H-6, H-10, H-11), 6.93 (d, $J_{7,6}$ = 8.0 Hz, 1H, H-7), 6.11 (d, $J_{13,12}$ = 15.2 Hz, 1H, H-13), 6.04 (s, 2H, CH_2-2), 5.28 (s, 2H, CH_2-16), 3.92 (s, 3H, OCH_3); ^{13}C-NMR (100 MHz DMSO-d_6): δ 192.12, 165.62, 157.04, 155.79, 155.15, 148.31, 148.00, 145.99, 140.97, 130.36, 124.62, 123.37, 121.75, 119.01, 115.44, 114.78, 108.53, 105.74, 101.41, 69.29, 56.63; IR (KBr, cm^{-1}): 1696 (C=O), 1446 (C=C), 1232 (C–F), 1035 (C–O).

2-Oxo-2-(*p*-tolyl)ethyl (2*E*,4*E*)-5-(benzo[*d*][1,3]dioxol-5-yl) penta-2,4-dienoate (20). Yellow color; 78% yield; M.P. 186–188 °C; EI-MS *m*/*z* (% rel. abund.): 350 (M^+, 37), 285 (3), 201 (100), 172 (71), 119 (88); HREI-MS *m*/*z*: calcd for $C_{21}H_{18}O_5$[350.1154], found [350.1150]; ^{1}H-NMR (400 MHz, DMSO-d_6): δ_H 7.86 (d, $J_{2',3'} = J_{6',5'}$ = 8.0 Hz, 1H, H-2′, H-6′), 7.49 (ddd, $J_{12,11} = J_{12,13}$ = 14.4 Hz, $J_{12,10}$ = 3.4 Hz, 1H, H-12), 7.36 (d, $J_{3',2'} = J_{5',6'}$ = 8.0 Hz, 2H, H-3′, H-5′), 7.23 (s, 1H, H-4), 7.04 (ovp, 3H, H-6, H-10, H-11), 6.93 (d, $J_{7,6}$ = 8.0 Hz, 1H, H-7), 6.05 (d, $J_{13,12}$ = 15.2 Hz, 1H, H-13), 6.04 (s, 2H, CH_2-2), 5.49 (s, 2H, CH_2-16), 2.37 (s, 3H, CH_3); IR (KBr, cm^{-1}): 2897 (C–H), 1698 (C=O), 1446 (C=C).

2-Oxo-2-(4-(trifluoromethyl)phenyl)ethyl (2*E*,4*E*)-5-(benzo[*d*][1,3]dioxol-5-yl)penta-2,4-dienoate (21). White color; 76% yield; M.P. 178–179 °C; EI-MS *m*/*z* (% rel. abund.): 404 (M^+, 42), 201 (74),173 (100), 145 (24), 115 (28); HREI-MS *m*/*z*: calcd for $C_{21}H_{15}O_5F_3$ [404.0872], found [404.0866]; ^{1}H-NMR (400 MHz, DMSO-d_6): δ_H 8.16 (d, $J_{3',2'} = J_{5',6'}$ = 8.2 Hz, 1H, H-3′, H-5′), 7.94 (d, $J_{2',3'} = J_{6',5'}$ = 8.3 Hz, 2H, H-2′, H-6′), 7.47 (ddd, $J_{12,11} = J_{12,13}$ = 15.2 Hz, $J_{12,10}$ = 3.0 Hz, 1H, H-12), 7.23 (s, 1H, H-4), 7.05 (ovp, 3H, H-6, H-10, H-11), 6.93 (d, $J_{7,6}$ = 8.0 Hz, 1H, H-7), 6.14 (d, $J_{13,12}$ = 15.2 Hz, 1H, H-13), 6.04 (s, 2H, CH_2-2), 5.58 (s, 2H, CH_2-16); ^{13}C-NMR (100 MHz DMSO-d_6): δ 192.68, 165.57, 148.34, 148.00, 146.26, 141.17, 137.13, 133.20, 132.94, 130.33, 130.25, 128.77, 128.66, 125.88, 124.58, 123.41, 118.71, 108.53, 105.74, 101.40, 66.54; IR (KBr, cm^{-1}): 1701 (C=O), 1447 (C=C), 1242 (C–F).

2-(2-Chlorophenyl)-2-oxoethyl (2*E*,4*E*)-5-(benzo[*d*][1,3]dioxol-5-yl)penta-2,4-dienoate (22). Light black color; 73% yield; M.P. 276–278 °C; EI-MS *m*/*z* (% rel. abund.): 370 (M^+, 33), 372 (M + 2, 12), 201 (100), 172 (84), 154 (9), 143 (26), 115 (43.9); HREI-MS *m*/*z*: calcd for $C_{20}H_{15}ClO_5$ [370.0608], found [373.0596]; ^{1}H-NMR (400 MHz, DMSO-d_6): δ_H 7.76 (dd, $J_{6',5'}$ = 7.5 Hz, 1H, H-6′), 7.57 (ovp, 2H, H-3′, H-5′), 7.49 (m, 1H, H-4′), 7.49 (ddd, $J_{12,11} = J_{12,13}$ = 15.2 Hz, $J_{12,10}$ = 2.0 Hz, 1H, H-12), 7.23 (s, 1H, H-4), 7.03

(ovp, 3H, H-6, H-10, H-11), 6.93 (d, $J_{7,6}$ = 8.0 Hz, 1H, H-7), 6.09 (d, $J_{13,12}$ = 15.2 Hz, 1H, H-13), 6.04 (s, 2H, CH_2-2), 5.32 (s, 2H, CH_2-16); ^{13}C-NMR (100 MHz DMSO-d_6): δ 195.41, 165.49, 148.37, 148.02, 146.37, 141.25, 134.99, 133.19, 130.70, 130.34, 129.75, 127.45, 124.58, 123.47, 118.57, 108.56, 105. 76, 101.43, 67.76; IR (KBr, cm^{-1}): 1700 (C=O), 1446 (C=C), 755 (C–Cl).

2-(3-Bromophenyl)-2-oxoethyl (2*E*,4*E*)-5-(benzo[*d*][1,3]dioxol-5-yl)penta-2,4-dienoate (23). Yellow color; 68% yield; M.P. 143–145 °C; EI-MS *m*/*z* (% rel. abund.): 414 (M^+, 22), 416 (M + 2, 21), 217 (3), 201 (89), 185 (17), 172 (100), 115 (48); HREI-MS *m*/*z*: calcd for $C_{20}H_{15}O_5Br$ [414.0103], found [414.0087]; ^{1}H-NMR (500 MHz, DMSO-d_6): δ_H 8.11 (t, $J_{2'(4',6')}$ = 1.6 Hz, 1H, H-2′), 7.94 (d, $J_{6',5'}$ = 7.8 Hz, 1H, H-6′), 7.90 (dd, $J_{4',5'}$ = 8.0 Hz, $J_{4',2'}$ = 1.0 Hz, 1H, H-4′), 7.54 (t, $J_{5'(4',6')}$ = 8.0 Hz, 1H, H-4′), 7.47 (ddd, $J_{12,11}$ = $J_{12,13}$ = 15.2 Hz, $J_{12,10}$ = 2.6 Hz, 1H, H-12), 7.25 (d, $J_{4,6}$ = 1.3 Hz, 1H, H-4), 7.06 (ovp, 3H, H-6, H-10, H-11), 6.94 (d, $J_{7,6}$ = 8.0 Hz, 1H, H-7), 6.14 (d, $J_{13,12}$ = 15.2 Hz, 1H, H-13), 6.05 (s, 2H, CH_2-2), 5.55 (s, 2H, CH_2-16); ^{13}C-NMR (100 MHz DMSO-d_6): δ 192.13, 165.59, 148.35, 148.02, 146.23, 141.16, 136.52, 135.93, 131.17, 130.34, 126.81, 124.61, 123.45, 122.27, 118.79, 108.56, 105.75, 101.43, 66.42; IR (KBr, cm^{-1}): 1702 (C=O), 1445 (C=C), 678 (C–Br).

2-(2-Iodophenyl)-2-oxoethyl (2*E*,4*E*)-5-(benzo[*d*][1,3]dioxol-5-yl)penta-2,4-dienoate (24). Brown color; 90% yield; M.P. 137–139 °C; EI-MS *m*/*z* (% rel. abund.): 434 (M^+, 89), 351 (13), 217 (100), 201 (20), 187 (24), 173 (37); HREI-MS *m*/*z*: calcd for $C_{19}H_{15}IO_4$ [434.0015], found [434.0002]; ^{1}H-NMR (400 MHz, DMSO-d_6): δ_H 7.90 (d, $J_{6',5'}$ = 7.8 Hz, 1H, H-6′), 7.46 (ovp, 3H, H-3′, H-5′, H-12), 7.22 (d, $J_{4,6}$ = 1.0 Hz, 1H, H-4), 7.13 (dt, $J_{4'(3',5')}$ = 7.6 Hz, $J_{4',6'}$ = 1.2 Hz, 1H, H-4′), 7.03 (ovp, 3H, H-6, H-10, H-11), 6.92 (d, $J_{7,6}$ = 8.0 Hz, 1H, H-7), 6.07 (d, $J_{13,12}$ = 14.6 Hz, 1H, H-13), 6.04 (s, 2H, CH_2-2), 5.12 (s, 2H, CH_2-16); IR (KBr, cm^{-1}): 1689 (C=O), 1449 (C=C), 608 (C–I).

2-(2-Nitrophenyl)-2-oxoethyl (2*E*,4*E*)-5-(benzo[*d*][1,3]dioxol-5-yl)penta-2,4-dienoate (25). White color; 78% yield; M.P. 230–232 °C; EI-MS *m*/*z* (% rel. abund.): 381 (M^+, 73), 201 (100), 173 (81), 115 (48); HREI-MS *m*/*z*: calcd for $C_{20}H_{15}O_7N$ [381.0849], found [381.0857]; ^{1}H-NMR (400 MHz, DMSO-d_6): δ_H 8.19 (d, $J_{3',4'}$ = 7.7 Hz, 1H, H-3′), 7.93 (t, $J_{4'(3',5')}$ = 7.0 Hz, 1H, H-4′), 7.83 (dt, $J_{5'(4',6')}$ = 8.9 Hz, $J_{5',3'}$ = 1.28 Hz, 1H, H-5′), 7.39 (ddd, $J_{12,11}$ = $J_{12,13}$ = 15.2 Hz, $J_{12,10}$ = 2.0 Hz, 1H, H-12), 7.24 (d, $J_{4,6}$ = 1.2 Hz, 1H, H-4), 7.03 (ovp, 3H, H-6, H-10, H-11), 6.94 (d, $J_{7,6}$ = 8.0 Hz, 1H, H-7), 6.05 (s, 2H, CH_2-2), 6.01 (d, $J_{13,12}$ = 15.2 Hz, 1H, H-13), 5.24 (s, 2H, CH_2-16); IR (KBr, cm^{-1}): 1698 (C=O), 1494 (N=O), 1449 (C=C).

Protocols for *in vitro* biological assays

α-Glucosidase inhibition assay and kinetic studies. α-Glucosidase from *Saccharomyces cerevisiae* inhibition assay was determined spectrophotometrically.[30,31]

The α-glucosidase inhibition percentage was calculated as follows:

$$\alpha\text{-glucosidaseinhibition } (\%) = [(A_{control} - A_{sample})/A_{control}] \times 100$$

where $A_{control}$ is the activity of the enzyme without compound/standard, and A_{sample} is the activity of the enzyme with compound/standard at different concentrations. The concentration of the inhibitor required to inhibit 50% of enzyme activity under the assay conditions was defined as the IC_{50}. The more active compounds **10**, **13**, **14**, and **17–19**, compared with acarbose, were further studied to determine the type of α-glucosidase inhibition and to conduct kinetic studies. Enzyme activity was determined using 4-pNPG as a substrate in buffer (pH 6.8). In the reaction media, the substrate concentrations were 0.20, 0.40, 0.80, 1.6, and 2.4 mg mL^{-1} in buffer (pH 6.8) containing enzyme (20 U mL^{-1}), with or without inhibitor. Increasing concentrations of 4-*p*NPG (0.20–2.4 mg mL^{-1}) and 5 μL of 20 U mL^{-1} α-glucosidase enzyme were added to a test tube, and the mixture was incubated at 25 °C for 14 min. The absorbance was measured at 405 nm. The obtained data were plotted as 1/activity (1/*V*) against 1/substrate concentration (1/[*S*]), according to the Lineweaver–Burk graph.[32] The Lineweaver–Burk graphs were used to obtain K_m and V_{max} values, and inhibition patterns were evaluated.

α-Amylase inhibitory activity and kinetic studies. Inhibition of α-amylase activity was performed as previously described.[30,31,33]

The α-amylase inhibition percentage was calculated as follows:

$$\alpha\text{-Amylase inhibition } (\%) = [(A_{control} - A_{sample})/A_{control}] \times 100$$

where $A_{control}$ is the activity of the enzyme without compound/standard, and A_{sample} is the activity of the enzyme with compound/standard at different concentrations. The concentration of the inhibitor required to inhibit 50% of enzyme activity under the assay conditions was defined as the IC_{50}. The more active compounds **10** and **17–19** than acarbose were further studied to determine the type of α-amylase inhibition. The enzyme activity was determined by using starch solution (increasing concentrations of starch solution (0.30–1.2 mg mL^{-1}) as a substrate in 0.02 M sodium phosphate buffer (pH 6.9). In the reaction media, the substrate concentrations were 0.30, 0.40, 0.60, 0.80, and 1.2 mg mL^{-1} in buffer (pH 6.9) containing enzyme, with or without inhibitor. The absorbance was measured at 540 nm, as written in the activity section above. The obtained data were plotted as 1/activity (1/*V*) against 1/substrate concentration (1/[*S*]), using a Lineweaver–Burk plot. The Lineweaver–Burk graphs were obtained, K_m and V_{max} values were calculated, and inhibition patterns were evaluated.

Cholinergic enzymes (AChE and BChE) inhibition studies. Acetylcholinesterase (AChE, E.C.3.1.1.7, from electric eel) and butyrylcholinesterase (BChE, E.C.3.1.1.8, from equine serum) were purchased from Sigma-Aldrich (Steinheim, Germany). All newly synthesized compounds were evaluated for cholinesterase (AChE and BChE) inhibition activity according to the reported protocol.[34,35] AChE and BChE enzyme solutions were prepared in a 1% gelatin solution at a concentration of 2.5 units per mL. AChE or BChE (50 μL), different concentrations of the tested compounds (50 μL), and acetylthiocholine chloride (ATC, 20 μL, 75 mM) or butrylthiocholine chloride (BTC, 20 μL, 75 mM) as substrate, were added to 1500 μL phosphate buffer (pH 8.0, 0.1 M) and incubated at 25 °C for 20 min. After the process

had been initiated, chromatographic reagent 5,5-dithio-*bis*(2-nitrobenzoic) acid (DTNB, 100 μL, 10 mM) was added to the enzyme-inhibitor mixture. After 20 min at 37 °C of yellow anion generation, a UV/Vis spectrophotometer was used to determine the absorbance at 412 nm. It was determined by preparing an identical solution of the enzyme in the absence of the tested compounds (as a control). All operations were repeated three times. The IC_{50} value was determined by linear regression of percent inhibition *versus* sample concentration in Excel. Donepezil chloride was used as a standard, and the results were compared. The cholinesterase inhibition percentage was calculated as follows:

$$\text{AChE} \cup \text{BChE inhibition}\ (\%) = [(A_{\text{control}} - A_{\text{sample}})/A_{\text{control}}] \times 100$$

The more active compounds **5**, **6**, and **8–11**, compared with the standard (donepezil chloride), were further studied to determine the types of AChE and BChE inhibition. In the reaction media, the different substrate (ATC or BTC) concentrations were 0.25, 0.5, 0.75, 1.0, and 1.5 mM in buffer (pH 8.0) containing the enzyme solution, with or without the inhibitor. Lineweaver–Burk graphs were obtained, K_m and V_{max} values were calculated, and inhibition patterns were evaluated to determine the inhibition type of these compounds on AChE and BChE.

Molecular docking methodology. Molecular docking studies were performed to evaluate the binding modes of the alkyl and aryl piperatederivatives against α-amylase and α-glucosidase. For this purpose, the crystal structures of human pancreatic α-amylase, α-glucosidase, AChE, and BChE with PDB IDs 1B2Y, 3WY1, 7E3H, and 5DYW, respectively, were downloaded from the Research Collaboratory for Structural Bioinformatics Protein Data Bank (RCSB PDB). The downloaded protein structures were checked for missing residues, which were corrected along with bond orders, while formal charges were assessed and corrected. The newly synthesized compound structures were created using the builder module, and the charges on compounds were minimized using the Merck Molecular Force Field 94×. These compounds were then subjected to molecular docking against the already prepared protein structures using the Molecular Operating Environment (MOE) software.

For molecular docking, the Triangle Matcher method was used as the primary placement method for docking, while LondondG was implemented as the placement scoring method. 'Induced fit receptor' algorithm was used for the refinement of the 50 generated poses, out of which the top 10 poses scored *via* GBVI/WSA dG method were used for further analysis. The binding poses of the top-ranked compounds were then analyzed using the Protein Ligand Interaction Profiler (PLIP), and the crucial interactions were noted.

Methodology

To further investigate the structural stability and conformational dynamics of the docked protein-ligand structures, all-atom molecular dynamics simulations[36] were performed using the CUDA-accelerated GROMACS (version 2024.1).[37] The force field AMBER99SB-ILDN[38] was applied for the protein topology, and the corresponding ligand parameters were generated using the ACPYPE server.[39] Subsequently, the catenated systems of the defined proteins, together with their selected alkyl and aryl piperate compounds, were solvated using the explicit water model TIP3P in a cuboid box, ensuring a 1.0 nm distance between the solute and the box edges.[40] Appropriate counterions were added to neutralize the system. Periodic boundary conditions in three dimensions were applied to mitigate the unphysical edge effects. Using the steepest descent algorithm, all systems underwent an energy-minimization step to remove potential steric clashes caused by additional ions and solvent, with a convergence threshold of 1000 kJ mol^{-1} nm^{-1}. Following the minimization step, the system temperature was increased from 0 to 300 K in an NVT ensemble. To equilibrate the system at 300 K and 1 bar, an NPT ensemble (isothermal-isobaric) was used. Simulations for heating, constant-pressure application, and the equilibrium-maintenance process were then performed for 1000 ps (1 ns) in each case using the modified Berendsen algorithm.[41] Finally, the systems were subjected to an MD production run of 100 ns under the conditions above defined to collect the necessary standard metrics data, such as root mean square deviation (RMSD), root mean square fluctuation (RMSF), and radius of gyration (RoG), required for the assessment of system structural stability, conformational deviations, flexibility, and protein compactness. Xmgrace server[42] was used to plot the graphs.

Antioxidant activity

Antioxidant activities and radical scavenging properties of the synthetic compounds were clarified using various *in vitro* antioxidant assays, including CUPRIC reducing antioxidant capacity (CUPRAC), ferric reducing antioxidant power (FRAP) assay, and DPPH (1,1-diphenyl-2-picrylhydrazyl) assays.

CUPric reducing antioxidant capacity (CUPRAC) assay

The CUPric reducing antioxidant capacity of the synthetic compounds was determined according to the literature.[43,44] Trolox® (Sigma Chemical Co., USA) was tested under the same conditions as a standard antioxidant compound, and the standard curve was linear between 8 mg mL^{-1} and 0.03125 mg mL^{-1} ($r^2 = 0.9987$). CUPRAC values were expressed as mM Trolox equivalents of 1 mg of the synthetic compound.

Ferric reducing antioxidant power (FRAP) assay

The ferric reducing antioxidant power (FRAP) assay was used to determine total antioxidant capacity. The FRAP reagent used was made by mixing 25 mL of acetate buffer (300 mM, pH 3.6) with 2.5 mL of 10 mM TPTZ solution in 40 mM HCl and 2.5 mL of 20 mM $FeCl_3 \cdot 6H_2O$ solution.[43,44] $FeSO_4 \cdot 7H_2O$ was used as a positive control to construct a reference curve at six different concentrations (15.63, 31.25, 62.5, 125, 250, 500, 1000 μM, $r^2 = 0.998$). FRAP values were expressed as mM $FeSO_4 \cdot 7H_2O$ equivalent per milligram of the compound, calculated as the $FeSO_4 \cdot 7H_2O$ concentration from the graph corresponding to the absorbance observed with the sample.

DPPH-free radical scavenging assay

The 1,1-diphenyl-2-picrylhydrazyl (DPPH) radical has been widely used in the model system to investigate the scavenging activities of several synthetic and natural compounds. The DPPH radical scavenging activity of the synthetic compounds was measured using the literature method.[43–45] Radical scavenging activity was measured using ascorbic acid as the standard, and all values are expressed as SC_{50} (μg compound per mL), the concentration of the sample required to cause 50% scavenging of the DPPH radical. The DPPH radical stock solution was prepared fresh daily. Butylated hydroxytoluene (BHT) was used as a positive radical scavenger molecule in the DPPH method. All determinations were carried out three times.

Pharmacokinetic and drug-likeness properties prediction

The pharmacokinetic and drug-likeness properties of the synthesized compound were predicted using the PreADME and SwissADME online servers. The SMILES notation of all active compounds was entered to assess Lipinski's Rule of Five for drug-likeness assessment. In addition, absorption-related parameters, including Caco-2 cell permeability, human intestinal absorption (HIA), blood–brain barrier (BBB) permeability, and skin permeability ($\log K_p$), were predicted to estimate the compound's oral and dermal bioavailability potential. Water solubility was determined using ESOL. XLOGP3-estimated lipophilicity, and the oral bioavailability score (F) were calculated to predict the likelihood of achieving sufficient systemic exposure. Structural alerts indicating potential assay interference were assessed through PAINS (pan-assay interference compounds) and Brenk filters. Finally, the synthetic accessibility score was generated to evaluate the ease of chemical synthesis, providing an overall prediction of the compound's feasibility as a drug-like candidate.[46,47]

Results and discussion

Chemistry

A series of twenty-four (24) alkyl and aryl piperate derivatives (**2–25**), including piperic acid, were synthesized in two reaction steps. In the first step, piperine was refluxed with 10% ethanolic KOH for 4–6 hours. After completion, the reaction mixture was acidified with dilute HCl, forming a precipitate, which was filtered and washed with distilled water to obtain piperic acid (**2**). In the second step, the piperic acid was reacted with various alkyl and aryl halides in acetonitrile using triethylamine as a base. The progress of both reactions was monitored by TLC (hexane : EtOAc, 3 : 7). The structures of the synthesized derivatives were confirmed by various spectroscopic techniques. To the best of our knowledge, out of twenty-four compounds, only piperic acid **2**,[25] compounds **4** and **20** (ref. 28 and 29) are structurally new derivatives (Scheme 1).

Spectral interpretation of new compound 3

In the EI-MS spectrum of derivative **3**, the molecular ion [M^+] was detected at *m*/*z* 257.2. The base peak, corresponding to the (*E*)-prop-1-en-1-ylbenzene cation, appeared at *m*/*z* 115.1, while additional fragment peaks were observed at *m*/*z* 217, 201, and 173. High-resolution EI-MS (HREI-MS) further confirmed the molecular formula, showing a calculated mass of 257.0688 and an observed mass of 257.0699, consistent with $C_{14}H_{11}NO_4$. A detailed fragmentation pattern is illustrated in Fig. 1a.

In the ^{1}H-NMR spectrum, the most downfield resonance was observed for H-7, appearing as a doublet at δ 8.04 with *ortho*-coupling to H-6 (J = 8.04 Hz). H-4 appeared as a doublet at δ 7.24, exhibiting *meta*-coupling with H-6 (J = 1.04 Hz). Overlapping signals for H-6, H-10, and H-11 were detected at δ 7.21. The dienone chain protons, H-12 and H-13, resonated at δ 7.51 and δ 6.07, respectively. Additionally, the methylene protons CH_2-2 and CH_2-16 appeared as singlets at δ 6.05 and δ 6.03 (Fig. 1b).

Compounds **1–25** were evaluated for their inhibitory activities against α-amylase and α-glucosidase, with results compared to the standard drug acarbose, which showed IC_{50} values of 14.87 ± 0.01 μM and 16.04 ± 0.01 μM for α-amylase and α-glucosidase, respectively. Piperic acid **2** (IC_{50} = 0.95 ± 0.01; 2.56 ± 0.01 μM) was recognized as the most potent, and derivative **5** showed the least inhibitory activity (IC_{50} = 44.56 ± 0.03; 45.28 ± 0.02 μM) against both enzymes. All compounds **1–25** were further evaluated for their inhibitory potential against AChE and BChE, and the results were compared with the reference drug donepezil chloride, which exhibited IC_{50} values of 38.97 ± 0.02 μM for AChE and 40.06 ± 0.02 μM for BChE. Amongst all derivatives, **13** ((IC_{50} = 0.36 ± 0.01; 2.57 ± 0.01 μM) was found to show remarkable inhibitory potential, while **24** showed the least activity (IC_{50} = 51.23 ± 0.03; 52.19 ± 0.02 μM) against AChE and BChE enzymes, respectively (Table 1).

Structure–activity relationship (SAR) of α-glucosidase and α-amylase inhibitory activities

The SAR analysis highlights a clear impact of structural modifications on inhibitory activity against α-glucosidase and α-amylase. The natural product piperine **1**, which is also the starting material, showed moderate activity (26.16 ± 0.02 μM for α-glucosidase; 24.87 ± 0.02 μM for α-amylase), weaker than the standard inhibitor (14.87 ± 0.01 μM for α-glucosidase; 16.04 ± 0.01 μM for α-amylase). Piperine **1** was transformed into piperic acid **2**, which showed a dramatic increase in potency (0.95 ± 0.01 μM for α-glucosidase; 2.56 ± 0.01 μM for α-amylase), making it significantly more active than the standard, likely due to stronger hydrogen bonding or ionic interactions at the active site. Subsequently, piperic acid was converted to various alkyl piperate derivatives **3–5**, which led to variable activities depending on the R group. Derivative **3** with an acetonitrile substituent showed increased inhibition (3.20 ± 0.02 μM for α-glucosidase; 9.32 ± 0.01 μM for α-amylase), much better than the standard, but less potent than its precursor, piperic acid. However, derivatives **4** and **5** with pentyloxy and butenyloxy substitutions exhibited weak activity (>40 μM for both enzymes), far less potent than the standard. These results emphasize that the free carboxylic acid moiety is crucial for strong enzyme binding. At the same time, bulky or hydrophobic ester substituents diminish activity, possibly due to steric

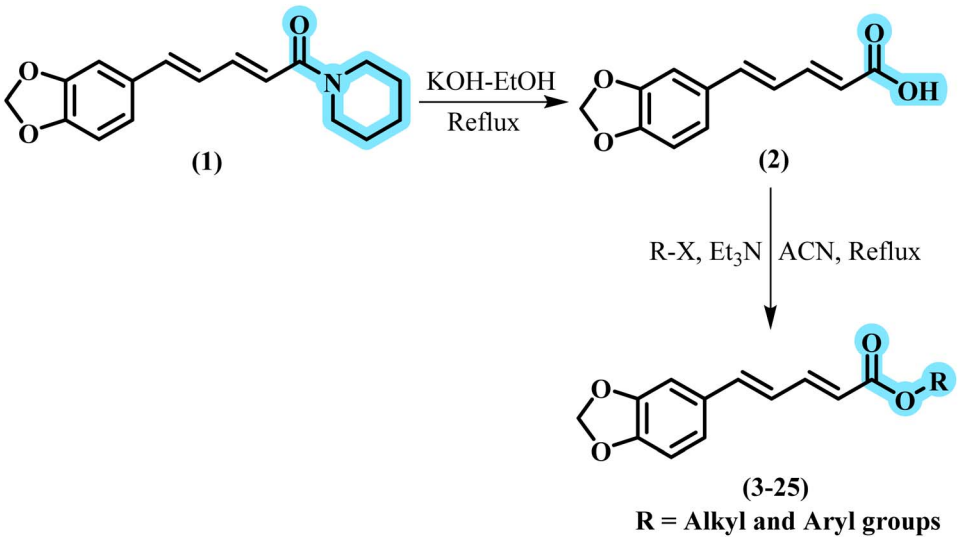

Scheme 1 Synthesis of alkyl and aryl piperate derivatives (3–25).

hindrance and reduced polar interactions. Overall, derivative **2** emerged as the most promising, clearly outperforming the standard inhibitor (Fig. 2).

The SAR analysis of derivatives **6–17**, each bearing diverse benzyloxy substitutions, highlights the critical influence of electronic and steric effects on inhibitory activity against α-glucosidase and α-amylase. Among all derivatives, **17** with a 3-methoxy benzyloxy substitution exhibited the highest potency (8.31 ± 0.01 μM for α-glucosidase; 11.75 ± 0.01 μM for α-amylase), suggesting that the electron-donating methoxy group at the *meta* position significantly enhances binding, possibly by improving π–π stacking or hydrogen bonding interactions within the enzyme active site. Derivative **6** with a 4-bromo substituent showed inhibitory potential (16.45 ± 0.03 μM for α-

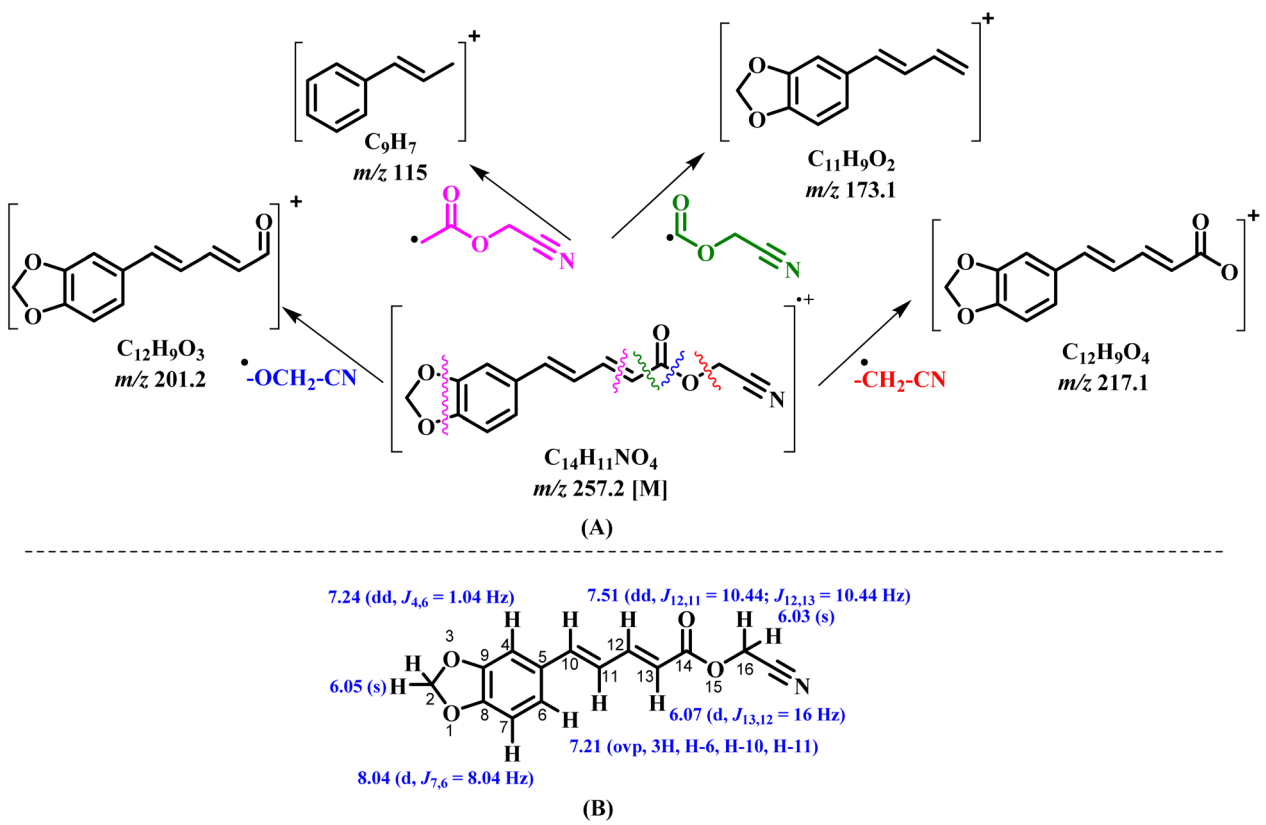

Fig. 1 (A) Plausible fragmentation pattern in EIMS; (B) ^{1}H-NMR chemical shifts of derivative **2**.

Table 1 α-Glucosidase, α-amylase, AChE, BChE inhibitory and antioxidant (CUPRAC, FRAP, DPPH methods) activities results of compounds **1–25**

		Enzyme inhibitory activities				Antioxidant activities		
Comp. No.	R	α-Glucosidase inhibitory activity $IC_{50} \pm SEM^a$	α-Amylase inhibitory activity $IC_{50} \pm SEM^a$	AChE inhibitory activity $IC_{50} \pm SEM^a$	BChE inhibitory activity $IC_{50} \pm SEM^a$	CUPRAC[f] method mean ± SD[b]	FRAP[g] method mean ± SD[b]	DPPH[h] method mean ± SD[b]
1	Piperine	26.16 ± 0.02	24.87 ± 0.02	40.16 ± 0.02	44.33 ± 0.02	6.83 ± 0.01	80.66 ± 0.16	165.25 ± 0.07
2	Piperic acid	0.95 ± 0.01	2.56 ± 0.01	44.78 ± 0.03	42.71 ± 0.02	6.12 ± 0.01	97.33 ± 0.21	189.12 ± 0.05
3	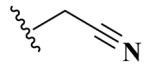	3.20 ± 0.02	9.32 ± 0.01	45.62 ± 0.03	47.62 ± 0.02	5.99 ± 0.01	98.45 ± 0.09	177.85 ± 0.06
4	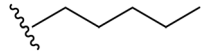	42.82 ± 0.03	43.44 ± 0.02	45.89 ± 0.03	44.22 ± 0.04	6.92 ± 0.01	109.00 ± 0.30	165.54 ± 0.07
5	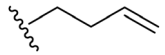	44.56 ± 0.03	45.28 ± 0.02	47.20 ± 0.03	49.34 ± 0.03	6.79 ± 0.01	110.25 ± 0.13	180.15 ± 0.07
6	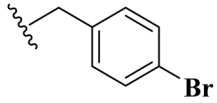	16.45 ± 0.03	17.56 ± 0.01	19.13 ± 0.01	31.72 ± 0.02	6 21 ± 0.01	97.56 ± 0.10	169.12 ± 0.05
7	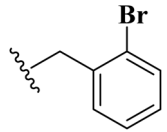	18.57 ± 0.02	17.24 ± 0.02	24.19 ± 0.02	38.92 ± 0.02	7.18 ± 0.01	116.08 ± 0.15	140.58 ± 0.05
8	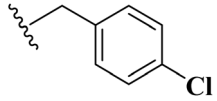	24.58 ± 0.03	26.17 ± 0.03	16.21 ± 0.01	29.78 ± 0.04	7.47 ± 0.01	97.75 ± 0.19	157.36 ± 0.08
9	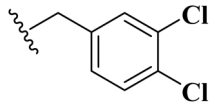	26.71 ± 0.02	27.52 ± 0.03	33.71 ± 0.02	40.95 ± 0.04	7.54 ± 0.01	94.00 ± 0.11	208.89 ± 0.05
10	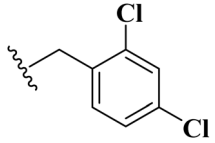	27.11 ± 0.02	26.14 ± 0.02	30.08 ± 0.02	40.89 ± 0.03	7.86 ± 0.01	91.50 ± 0.09	160.80 ± 0.97
11	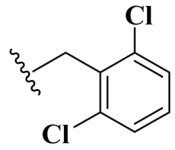	25.89 ± 0.02	26.96 ± 0.02	35.30 ± 0.02	45.37 ± 0.02	7.38 ± 0.01	107.33 ± 0.07	114.13 ± 0.06

Table 1 (*Contd.*)

Comp. No.	R	Enzyme inhibitory activities: α-Glucosidase inhibitory activity $IC_{50} \pm SEM^a$	Enzyme inhibitory activities: α-Amylase inhibitory activity $IC_{50} \pm SEM^a$	Enzyme inhibitory activities: AChE inhibitory activity $IC_{50} \pm SEM^a$	Enzyme inhibitory activities: BChE inhibitory activity $IC_{50} \pm SEM^a$	Antioxidant activities: CUPRAC[f] method mean ± SD[b]	Antioxidant activities: FRAP[g] method mean ± SD[b]	Antioxidant activities: DPPH[h] method mean ± SD[b]
12	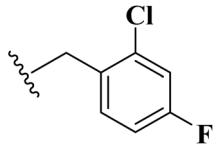	22.87 ± 0.02	23.78 ± 0.02	2.92 ± 0.009	10.76 ± 0.01	6.45 ± 0.01	93.58 ± 0.08	160.47 ± 0.06
13	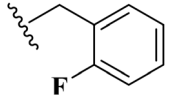	20.13 ± 0.03	22.12 ± 0.01	0.36 ± 0.01	2.57 ± 0.01	6.10 ± 0.01	87.33 ± 0.14	119.58 ± 0.07
14	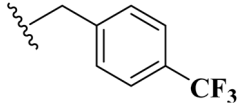	21.53 ± 0.02	21.97 ± 0.02	7.78 ± 0.02	18.56 ± 0.01	6.66 ± 0.01	104.83 ± 0.11	220.46 ± 0.08
15	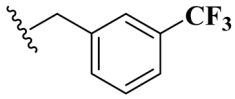	22.76 ± 0.03	21.76 ± 0.03	5.89 ± 0.01	15.13 ± 0.02	6.87 ± 0.01	105.25 ± 0.17	135.41 ± 0.08
16	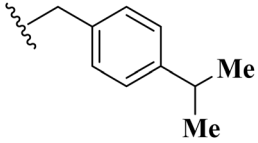	31.55 ± 0.02	32.18 ± 0.02	46.15 ± 0.02	44.27 ± 0.02	7.75 ± 0.01	85.25 ± 0.08	205.15 ± 0.05
17	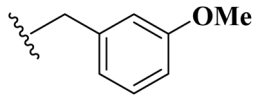	8.31 ± 0.01	11.75 ± 0.01	42.17 ± 0.03	41.38 ± 0.03	5.92 ± 0.01	81.50 ± 0.15	184.78 ± 0.08
18	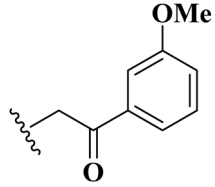	11.65 ± 0.01	14.02 ± 0.02	45.91 ± 0.03	44.26 ± 0.03	6.04 ± 0.01	98.58 ± 0.11	140.78 ± 0.06
19	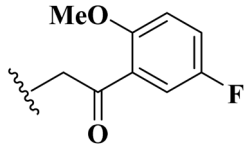	21.18 ± 0.03	20.71 ± 0.02	1.27 ± 0.01	6.89 ± 0.02	6.10 ± 0.01	91.50 ± 0.19	205.56 ± 0.09

Table 1 (*Contd.*)

Comp. No.	R	Enzyme inhibitory activities: α-Glucosidase inhibitory activity $IC_{50} \pm SEM^a$	α-Amylase inhibitory activity $IC_{50} \pm SEM^a$	AChE inhibitory activity $IC_{50} \pm SEM^a$	BChE inhibitory activity $IC_{50} \pm SEM^a$	Antioxidant activities: CUPRAC[f] method mean ± SD[b]	FRAP[g] method mean ± SD[b]	DPPH[h] method mean ± SD[b]
20	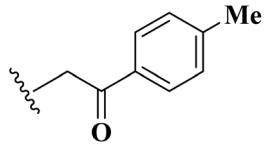	36.85 ± 0.03	35.45 ± 0.02	47.90 ± 0.03	51.76 ± 0.02	8.57 ± 0.01	126.08 ± 0.13	95.28 ± 0.04
21	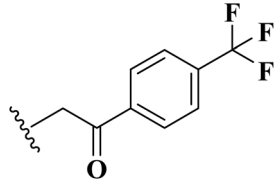	23.78 ± 0.04	22.13 ± 0.03	10.01 ± 0.02	21.93 ± 0.02	6.39 ± 0.01	95.25 ± 0.18	195.36 ± 0.07
22	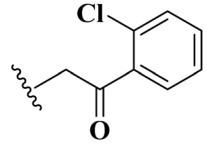	25.14 ± 0.03	23.19 ± 0.02	12.64 ± 0.01	27.25 ± 0.03	6.42 ± 0.02	86.08 ± 0.22	135.52 ± 0.08
23	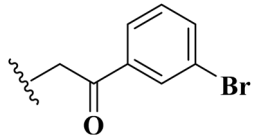	17.21 ± 0.01	16.89 ± 0.02	21.67 ± 0.02	36.41 ± 0.03	6.84 ± 0.03	105.25 ± 0.24	210.18 ± 0.04
24	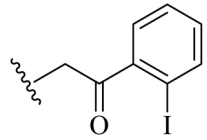	28.89 ± 0.03	30.43 ± 0.01	51.23 ± 0.03	52.19 ± 0.02	6.25 ± 0.01	107.33 ± 0.19	170.56 ± 0.08
25	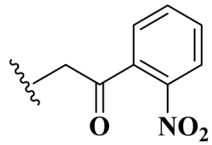	5.42 ± 0.01	6.81 ± 0.01	40.89 ± 0.03	42.52 ± 0.03	5.92 ± 0.01	86.08 ± 0.20	165.23 ± 0.06
Standards	Acarbose[c]	14.87 ± 0.01	16.04 ± 0.01	—	—	—	—	
	Donepezil chloride[d]	—	—	38.97 ± 0.02	40.06 ± 0.02	—	—	
	BHT[e]							65.11 ± 0.02

[a] SEM (standard error mean). [b] SD (standard deviation). [c] Acarbose (standard inhibitor for α-glucosidase and α-amylase inhibitory activities). [d] Donepezil chloride (standard inhibitor for AChE and BChE inhibitory activities). [e] BHT (butylated hydroxytoluene, standard for DPPH assay). [f] mM Trolox per mg compound. [g] μM $FeSO_4 \cdot 7H_2O$ per mg compound. [h] SC_{50} value, μM.

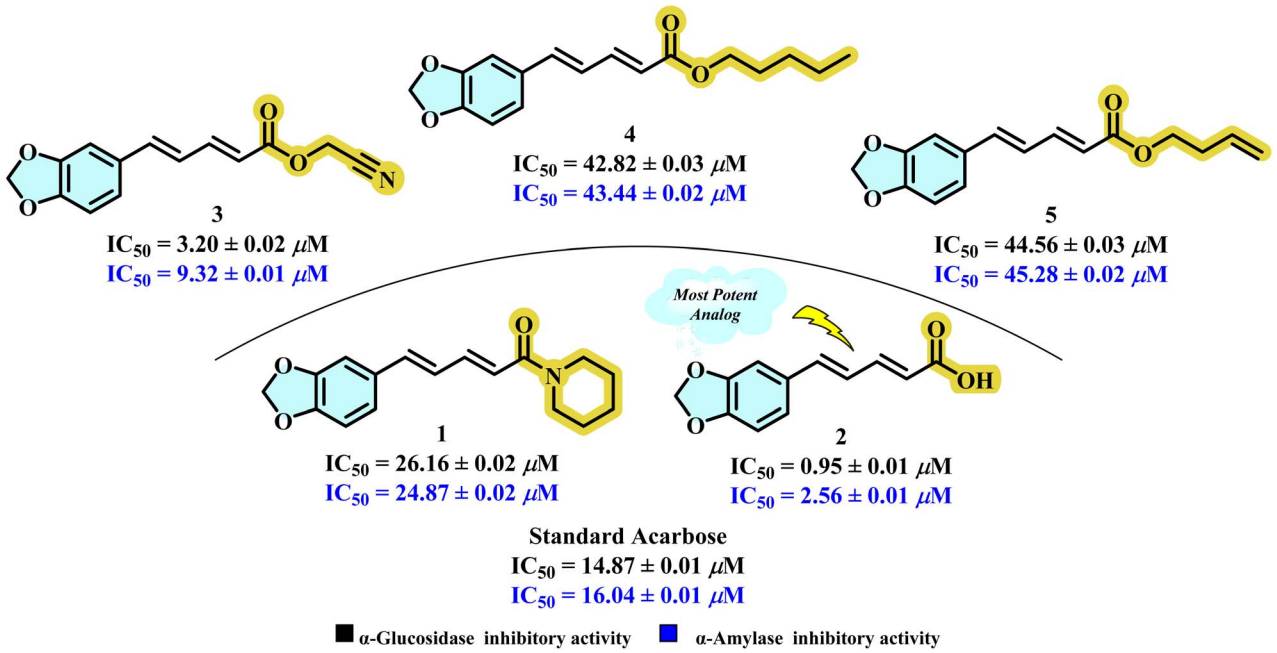

Fig. 2 SAR of piperine **1**, piperic acid **2**, and alkyl piperate **3–5** for α-glucosidase and α-amylase inhibitory activities.

glucosidase; 17.56 ± 0.01 μM for α-amylase), close to standard, indicating that the *para*-bromo group also favors binding, likely due to its balanced size and moderate electron-withdrawing nature. Derivative **7** with an *ortho*-bromo group showed slightly reduced activity (18.57 ± 0.02 μM for α-glucosidase; 17.24 ± 0.02 μM for α-amylase), indicating that *ortho* substitution may introduce steric hindrance, affecting binding affinity. Mono and dichloro-containing derivatives (**8–11**) displayed closed but moderate to lower activity (~24.58–27.11 μM) than standard acarbose, suggesting that chloro substitutions or their positions might reduce favorable interactions, likely due to increased steric bulk. Activity of derivative **10** (27.11 ± 0.02 μM for α-glucosidase; 26.14 ± 0.02 μM for α-amylase) can be compared with structurally similar derivative **12** (22.87 ± 0.02 μM for α-glucosidase; 23.78 ± 0.02 μM for α-amylase), which contains fluoro instead of chloro at the 4-position, showing improved inhibitory potential. This improvement may be attributed to the small size and high electronegativity of fluorine, which can facilitate hydrogen bonding. Similarly, 2-fluoro derivative **13** showed slightly improved activity (20.13 ± 0.03 μM for α-glucosidase; 22.12 ± 0.01 μM for α-amylase). Nonetheless, these compounds are still moderate inhibitors. Further, trifluoromethyl derivatives **14** and **15** also showed moderate activity (~21.53–22.76 μM), similar to other fluoro derivatives. Notably, derivative **16** with a bulky 4-isopropyl substituent showed weak activity (31.55 ± 0.02 μM for α-glucosidase; 32.18 ± 0.02 μM for α-amylase), highlighting that large alkyl groups introduce significant steric hindrance, reducing enzyme binding (Fig. 3). Overall, the data reveal that the electron-donating 3-methoxy group significantly enhances potency, whereas bulky or multiple halogen substitutions negatively impact activity.

SAR analysis of phenacyloxy derivatives **18–25** reveals notable effects of different substituents on enzyme inhibition. Among all, derivative **25** with a 2-nitro group exhibited the highest potency (5.42 ± 0.01 μM for α-glucosidase; 6.81 ± 0.01 μM for α-amylase), suggesting that a strong electron-withdrawing nitro group at the 2-position significantly enhances binding, possibly *via* stronger hydrogen bonding or favorable electrostatic interactions within the enzyme active site. Derivative **18** bearing a 3-methoxy substituent showed good activity (11.65 ± 0.01 μM for α-glucosidase; 14.02 ± 0.02 μM for α-amylase), highlighting that an electron-donating methoxy group at the *meta* position can also improve affinity, likely through favorable electronic effects. Derivative **23** with a 3-bromo substituent also showed relatively better activity (17.21 ± 0.01 μM for α-glucosidase; 16.89 ± 0.02 μM for α-amylase), indicating that moderate-sized halogens at the 3-position support reasonable enzyme interactions. Derivatives **19** (2-methoxy-5-fluoro), **21** (4-trifluoromethyl), and **22** (2-chloro) exhibited moderate activities (~21.18–25.14 μM), suggesting that more electronegative chloro and fluoro groups are not particularly favorable for inhibiting both enzymes. Derivative **24** with a larger 2-iodo group also showed weaker activity (28.89 ± 0.03 μM for α-glucosidase; 30.43 ± 0.01 μM for α-amylase), which might introduce steric hindrance, diminishing binding. In addition to this, derivative **20** with a 4-methyl substituent showed the weakest activity (36.85 ± 0.03 μM for α-glucosidase; 35.45 ± 0.02 μM for α-amylase), indicating that small alkyl groups at the 4-position reduce potency, likely due to a lack of strong electronic or hydrogen bonding contributions (Fig. 4). Overall, the SAR suggests that strong electron-withdrawing groups (*e.g.*, nitro) at the 2-position and electron-donating methoxy groups at the 3-position most favorably enhance

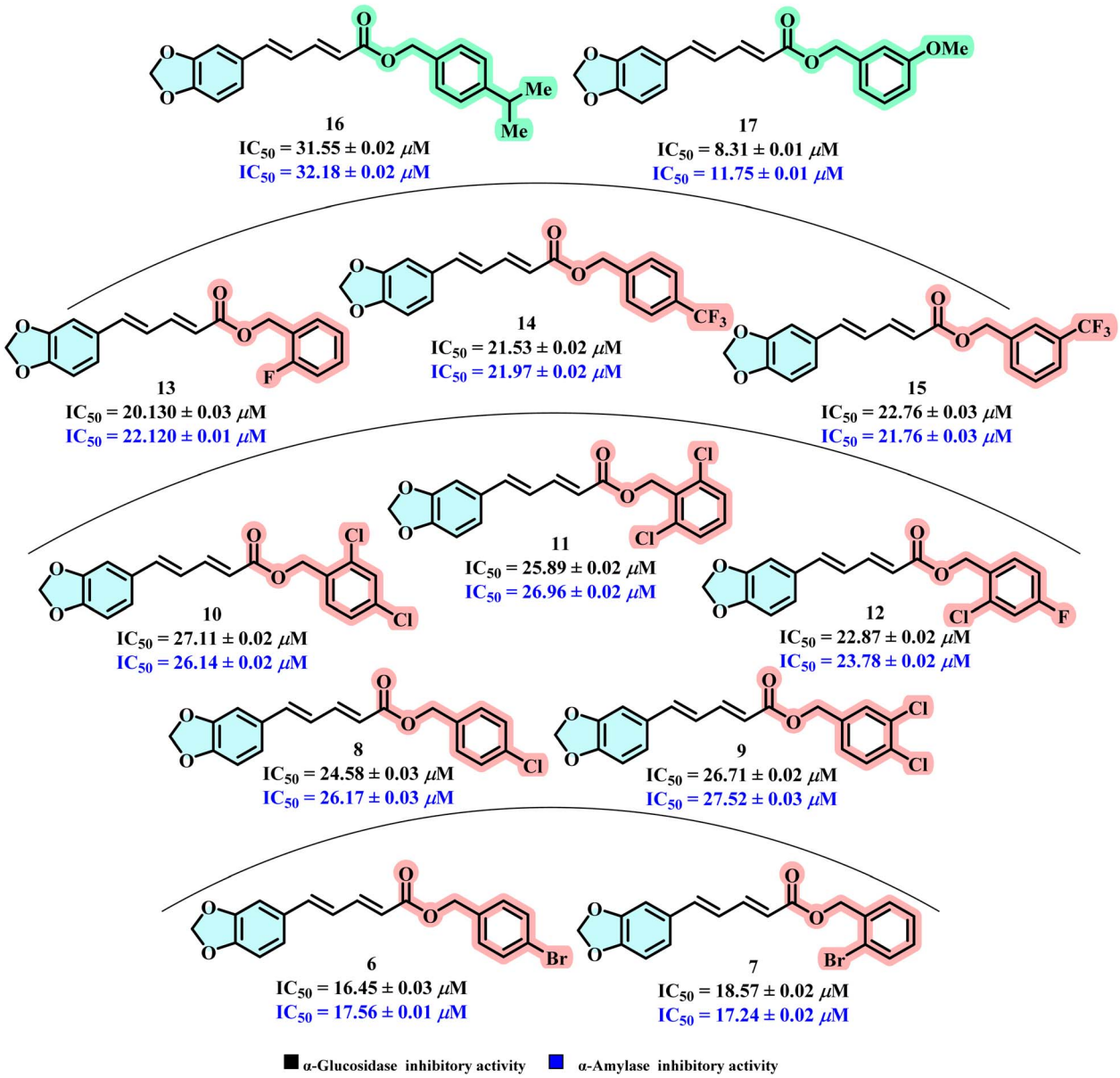

Fig. 3 SAR of benzyloxy-substituted piperate derivatives 6–17 for α-glucosidase and α-amylase inhibitory activities.

inhibitory activity, providing a clear guide for further optimization.

SAR of AChE and BChE inhibitory activities

SAR analysis highlights that derivatives **1–5** demonstrated inferior activity compared to the standard donepezil chloride (38.97 ± 0.02 μM for AChE; 40.06 ± 0.02 μM for BChE). The starting material, piperine **1**, exhibited slightly less potent (40.16 ± 0.02 μM for AChE; 44.33 ± 0.02 μM for BChE) activity than the standard. Surprisingly, conversion to the piperic acid **2** did not improve potency (44.78 ± 0.03 μM for AChE; 42.71 ± 0.02 μM for BChE), suggesting that introducing a free carboxyl group did not enhance binding affinity. Further transformation into ester derivatives (compounds **3–5**) also didn't improve activity. Derivative **3** with an acetonitrile substituent showed even less activity (45.62 ± 0.03 μM for AChE; 42.62 ± 0.02 μM for BChE) than piperic acid, indicating that introducing a polar, small group did not aid binding. Derivatives **4** and **5**, containing bulkier pentyloxy and butenyloxy groups, showed decreased activities (45.89–47.20 μM for AChE; 44.22–49.34 μM for BChE), suggesting that larger alkyl substituents increase steric hindrance and weaken interactions with the enzyme active site (Fig. 5).

The SAR analysis of derivatives **6–17**, compared to the standard inhibitor, demonstrates a clear influence of benzyloxy substituents on inhibitory activity. Derivative **13** with a 2-fluoro substituent showed exceptional potency (0.36 ± 0.01 μM for AChE; 2.57 ± 0.01 μM for BChE), highlighting that a small, strongly electron-withdrawing group at the 2-position significantly enhances enzyme binding, likely through improved

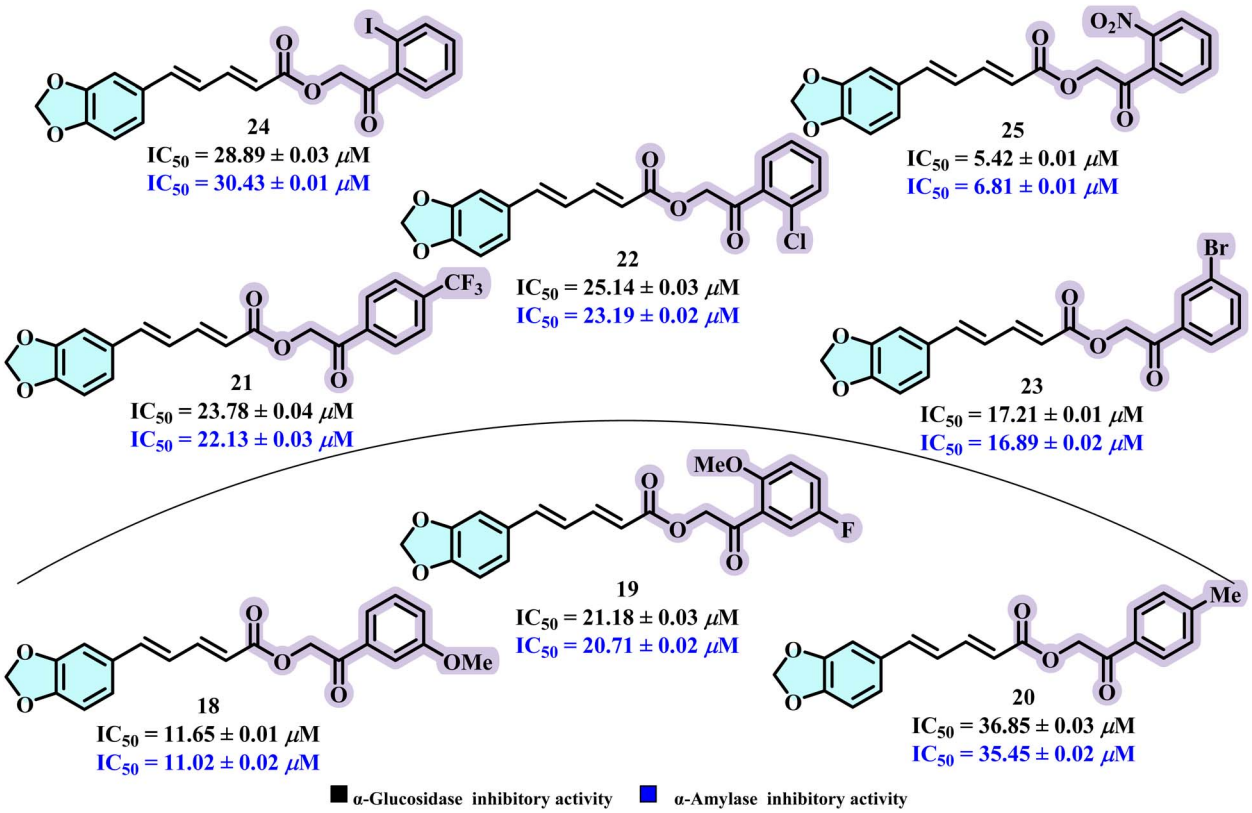

Fig. 4 SAR of phenacyloxy substituted piperate derivatives 18–25 for α-glucosidase and α-amylase inhibitory activities.

hydrogen bonding or strong dipolar interactions. Similarly, derivative **12** with 2-chloro-4-fluoro substituents also exhibited strong activity (2.92 ± 0.01 μM for AChE; 10.76 ± 0.01 μM for BChE), suggesting the effect of multiple electron-withdrawing substituents. Trifluoromethyl-substituted derivatives **14** and **15** also showed good activity (5.89–7.78 μM for AChE; 15.13–18.56 μM for BChE), reinforcing the notion that strong electron-withdrawing groups increase binding affinity, possibly by facilitating a better fit and interaction within the enzyme active site. Among chloro-substituted derivatives **8–11**, mono 4-chloro

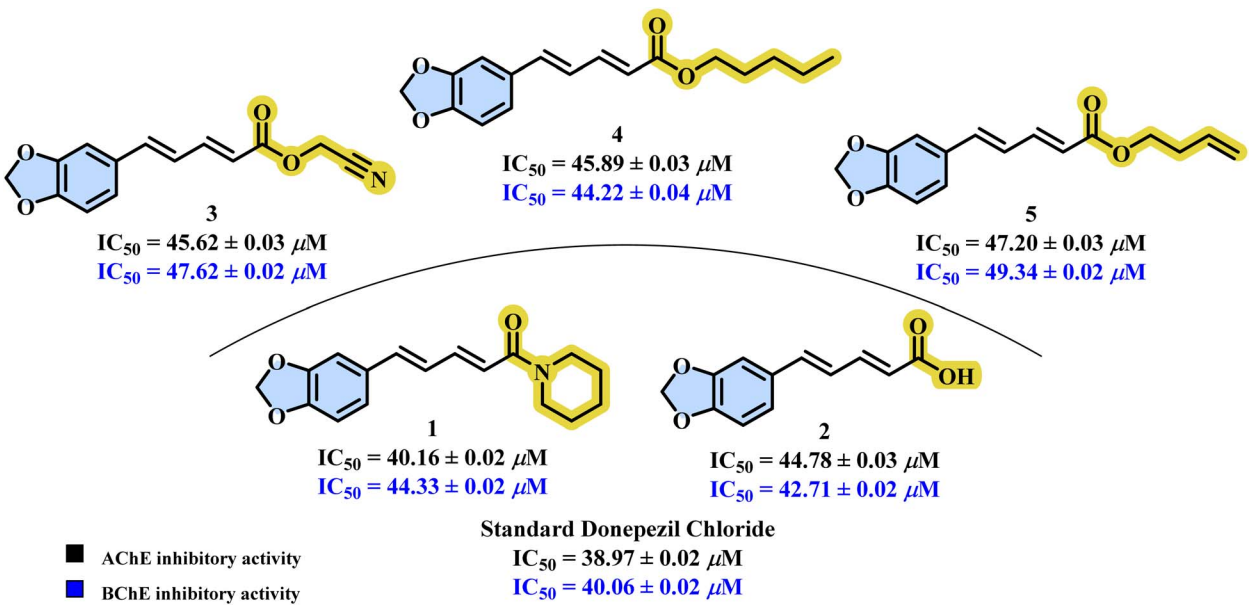

Fig. 5 SAR of piperine **1**, piperic acid **2**, and alkyl piperate **3–5** for AChE and BChE inhibitory activities.

bearing derivatives **8** (16.21 ± 0.01 μM for AChE; 29.78 ± 0.04 μM for BChE) showed activity better than the standard but less potent than fluoro-containing compounds. In contrast, dichloro derivatives **9–11** exhibited less potential than the mono-chloro derivative in the range of IC_{50} = 30.08–35.30 μM for AChE and 40.89–45.37 μM for BChE, likely due to steric hindrance and reduced flexibility in enzyme binding. Activity of derivative **8** was compared with **6** (19.13 ± 0.01 μM for AChE; 31.72 ± 0.02 μM for BChE), which only has bromo instead of chloro, and showed slightly less potential, likely due to increased size and steric hindrance. Moving bromo from the 4 to the 2 position in derivative 7 (24.19 ± 0.02 μM for AChE; 38.92 ± 0.02 μM for BChE) further decreased inhibitory activity, most probably due to increased steric hindrance. Derivatives **16** and **17** have 4-isopropyl and 3-methoxy substituents, respectively, but showed moderate activity, weaker than the standard, suggesting the bulky or electron-donating substituent disrupts optimal interactions (Fig. 6). Overall, the data strongly support that small electron-withdrawing substituents, especially fluorine, dramatically enhance potency.

SAR analysis of derivatives **18–25** reveals significant effects of phenacyloxy substituents on enzyme inhibition compared to donepezil chloride. Derivative **19**, with a 2-methoxy-5-fluoro substitution, showed the highest potency (1.27 ± 0.01 μM for

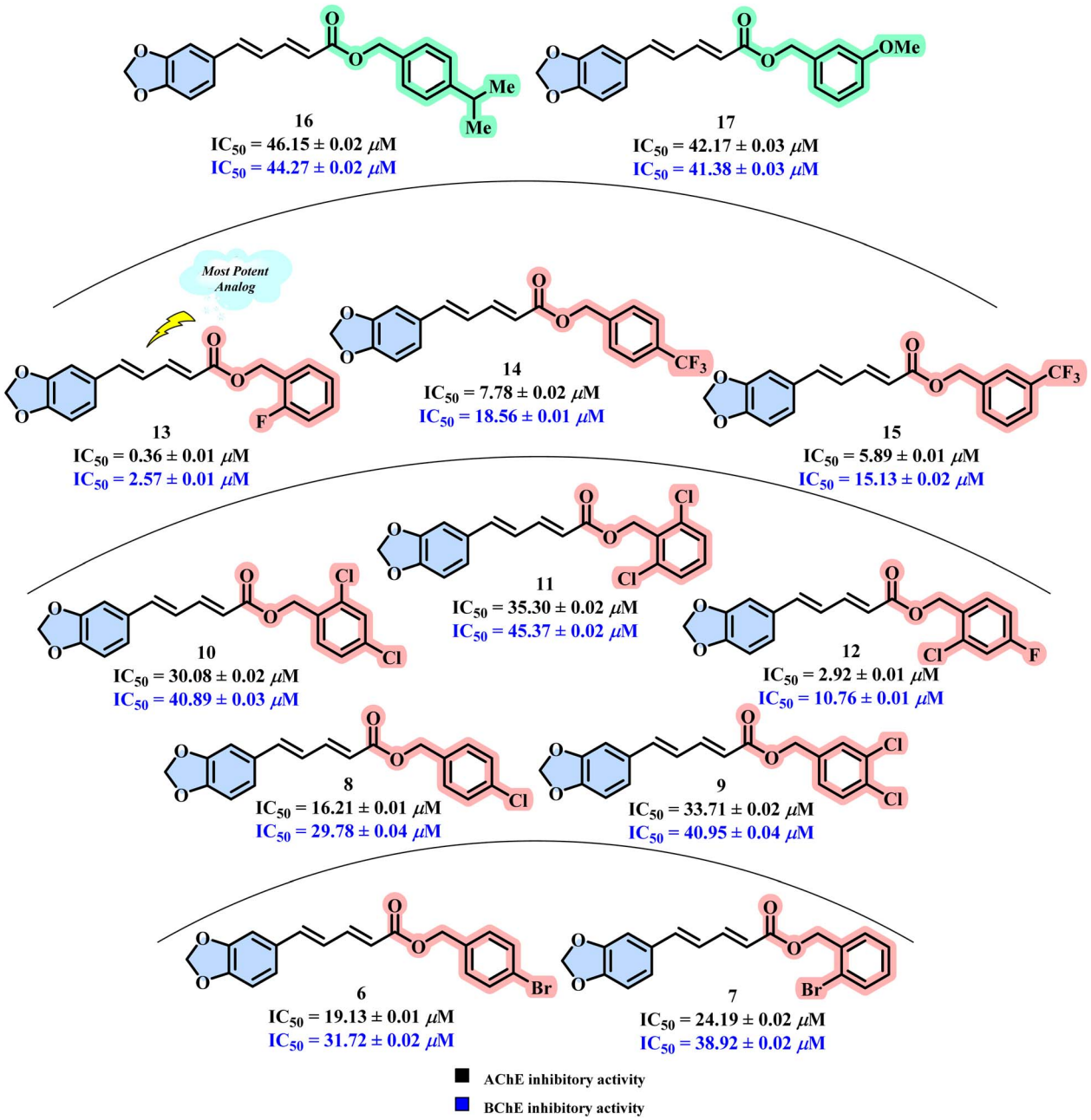

Fig. 6 SAR of benzyloxy substituted piperate derivatives **6–17** for AChE and BChE inhibitory activities.

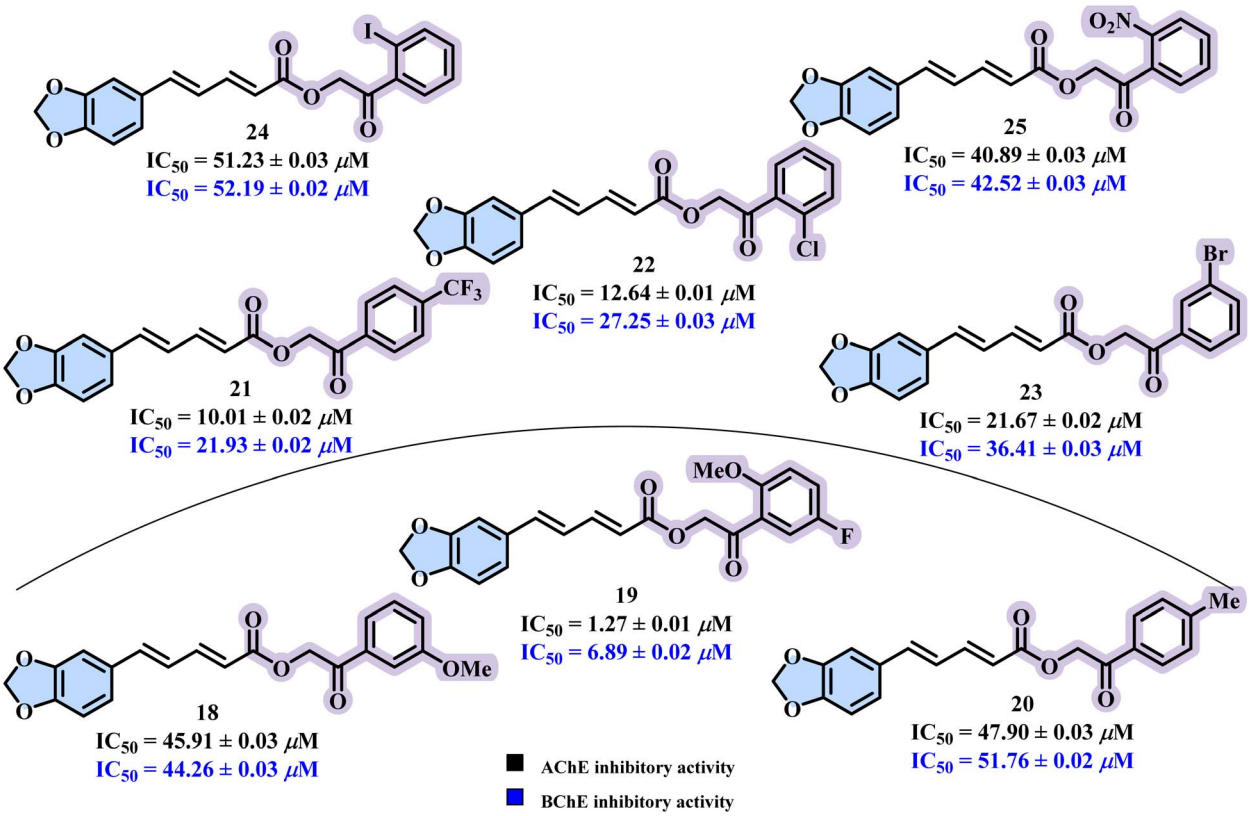

Fig. 7 SAR of phenacyloxy substituted piperate derivatives **18–25** for AChE and BChE inhibitory activities.

Table 2 Type of α-glucosidase and α-amylase inhibition in the presence of the compounds and acarbose, with some kinetic parameters, K_m and V_{max} values

	α-Glucosidase inhibitory activity				
	4-Nitrophenyl α-D-glucopyranoside				
Inhibitors	K_m (mg mL^{-1})	V_{max} (mM min^{-1})	Type of inhibition	IC_{50} (μM)	R^2
Control	0.46	185.00	—	—	0.991
Acarbose	0.53	185.00	Competitive	14.870	0.990
2	1.15	185.00	Competitive	0.950	0.988
3	0.94	185.00	Competitive	3.200	0.987
25	0.73	185.00	Competitive	5.420	0.990
17	0.33	140.40	Uncompetitive	8.310	0.985
18	0.39	163.10	Uncompetitive	11.650	0.989
	α-Amylase inhibitory activity				
	Starch				
Inhibitors	K_m (mg mL^{-1})	V_{max} (mM min^{-1})	Type of inhibition	IC_{50} (μM)	R^2
Control	0.62	265.00	—	—	0.996
Acarbose	0.76	265.00	Competitive	16.040	0.989
2	1.25	265.00	Competitive	2.560	0.985
25	1.03	265.00	Competitive	6.810	0.991
3	0.44	215.00	Uncompetitive	9.320	0.990
17	0.51	228.00	Uncompetitive	11.750	0.993
18	0.58	240.00	Uncompetitive	14.020	0.991

AChE; 6.89 ± 0.02 μM for BChE), indicating a strong synergistic effect of electron-donating methoxy and electron-withdrawing fluoro groups, possibly enhancing both hydrogen bonding and dipolar interactions. Derivatives **21** and **22** with 4-trifluoromethyl and 2-chloro substitutions also displayed good activity (10.01 ± 0.02 and 12.64 ± 0.01 μM for AChE; 21.93 ± 0.02 and 27.25 ± 0.03 μM for BChE), suggesting that electron-withdrawing substituents improve binding affinity. Derivative **23** (IC_{50} = 21.67 ± 0.02 μM for AChE; 36.41 ± 0.03 μM for BChE) with a 3-bromo group also showed better activity than donepezil chloride but weaker than the chloro derivative **22**. Similarly, derivative **24** with a 2-iodo substituent also exhibited the lowest activity (51.23 ± 0.03 μM for AChE; 52.19 ± 0.02 μM for BChE), suggesting that increasing the size of the halogen decreased inhibitory activity. In contrast, derivatives with only electron-donating substituents, such as **18** (45.91 ± 0.03 μM for AChE; 44.26 ± 0.03 μM for BChE) and **20** (47.90 ± 0.03 μM for AChE; 51.76 ± 0.02 μM for BChE) with 3-methoxy and 4-methyl groups, respectively, demonstrated comparatively weaker activities, implying these groups fail to promote effective interactions with the active site. Additionally, the only 2-nitro-substituted derivative, **25**, showed activity comparable to the standard (Fig. 7).

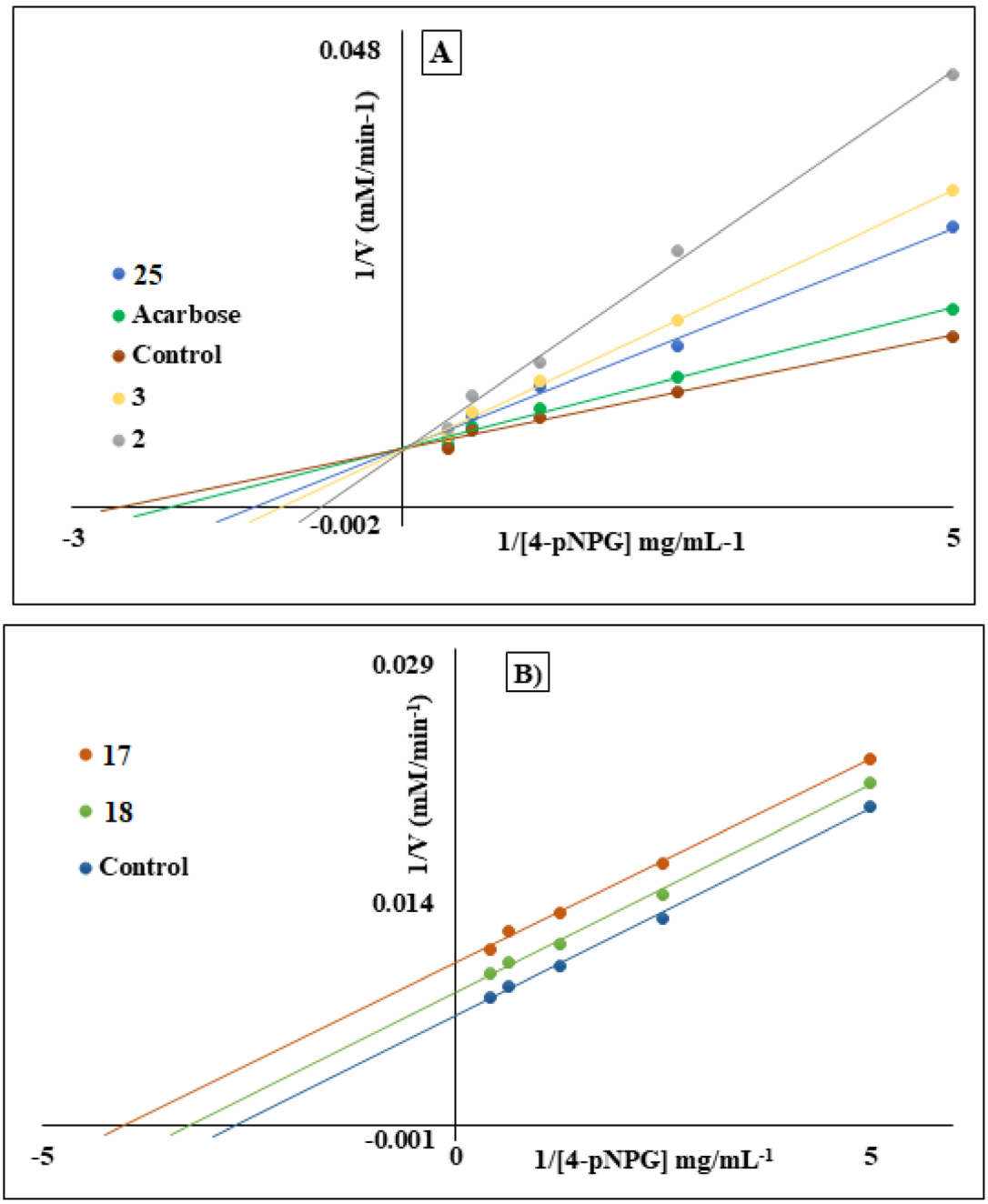

Fig. 8 Lineweaver–Burk plots of (A) acarbose and compounds **2**, **3**, and **25** showing competitive inhibition; (B) compounds **17** and **18** showing uncompetitive inhibition against α-glucosidase.

Kinetic studies on α-glucosidase and α-amylase enzymes

The synthesized compounds were evaluated for their α-glucosidase and α-amylase inhibitory activities by plotting percentage relative activities against inhibitor concentrations.

In case of α-glucosidase inhibition, out of all compounds, **2** exhibited the strongest inhibition, with an IC_{50} of 0.950 ± 0.004 μM, surpassing acarbose. The order of potency was: **2** > **3** > **25** > **17** > **18** > acarbose (Table 1). The inhibition type of compounds **2**, **3**, **25**, **17**, and **18** was determined using Lineweaver–Burk plots from assays with varying concentrations of 4-pNPG in the presence or absence of the inhibitors. Compounds **2**, **3**, and **25** showed increased K_m values with unchanged V_{max} (185.00 mM min^{-1}), indicating competitive inhibition, in which the inhibitors bind to the enzyme's active site and compete with the substrate. Among these, compound **2** had the highest affinity (K_m = 1.15 mg mL^{-1}). In contrast, compounds **17** and **18** exhibited decreases in both K_m and V_{max}, consistent with uncompetitive inhibition, where the inhibitor binds exclusively to the enzyme–substrate complex (Table 2 and Fig. 8A and B).

However, for α-amylase, the most potent inhibitors, in order of activity, were: **2** > **25** > **3** > **17** > **18** > acarbose (Table 1). Compound **2** showed the strongest inhibition, with an IC_{50} of

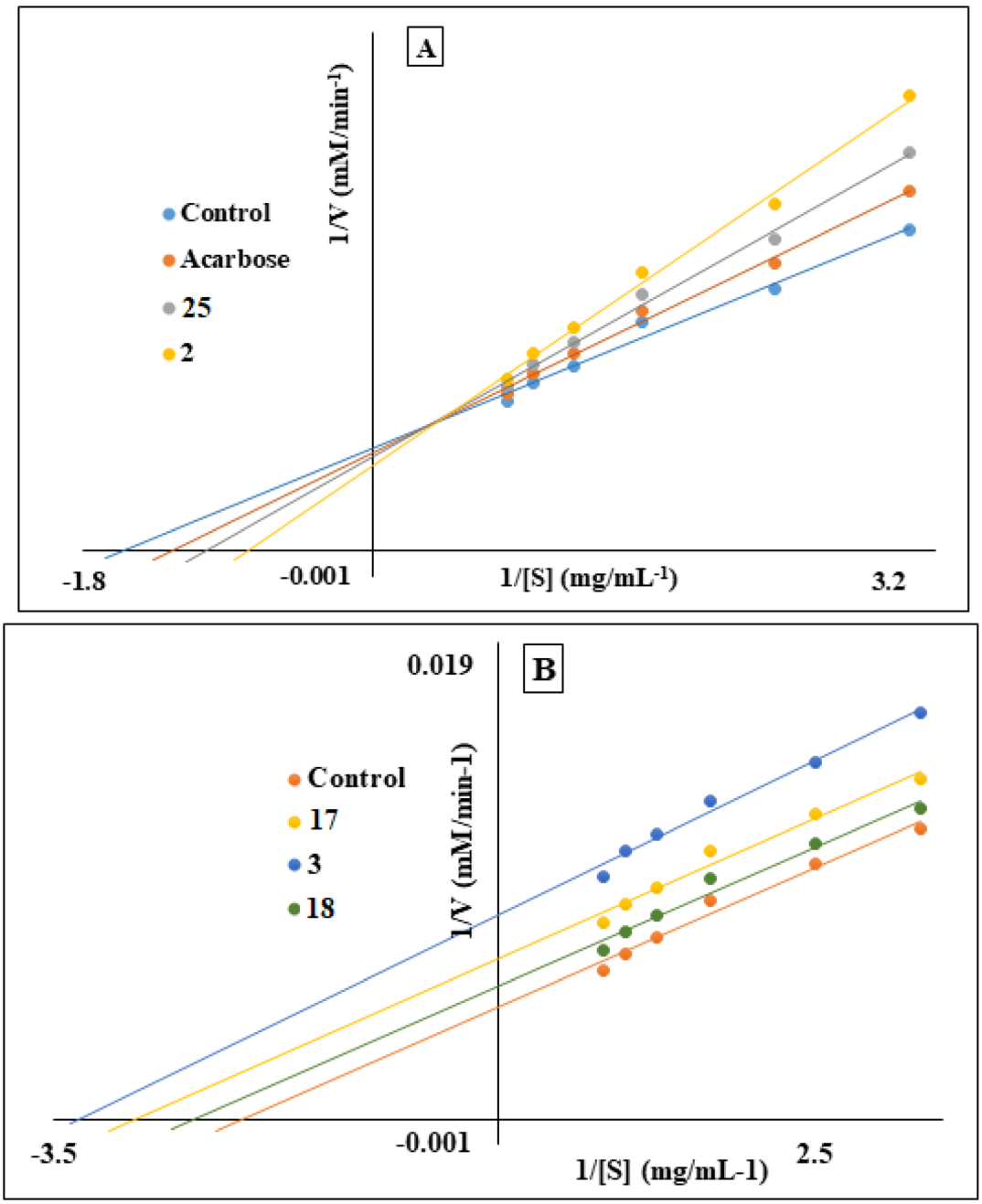

Fig. 9 Lineweaver–Burk plots of (A) acarbose and compounds **2** and **25** showing competitive inhibition; (B) compounds **3**, **17**, and **18** showing uncompetitive inhibition against α-amylase enzyme.

Table 3 Type of AChE and BChE inhibition of the compounds and donepezil, with their K_m and V_{max} values

	For AChE inhibitory activity				
	ATC				
Inhibitors	K_m (mM)	V_{max} (mM min^{-1})	Type of inhibition	IC_{50} (μM)	R^2
Control	0.89	190.00	—	—	0.992
Donepezil	1.03	190.00	Competitive	38.970	0.989
13	2.43	190.00	Competitive	0.360	0.994
19	2.09	190.00	Competitive	1.270	0.992
12	1.89	190.00	Competitive	2.920	0.990
15	1.72	190.00	Competitive	5.890	0.991
14	1.52	190.00	Competitive	7.785	0.994
21	1.41	190.00	Competitive	10.010	0.990
22	1.34	190.00	Competitive	12.640	0.995
8	1.14	190.00	Competitive	16.210	0.990
6	0.56	116.00	Uncompetitive	19.130	0.995
23	0.60	123.00	Uncompetitive	21.670	0.992
7	0.66	135.00	Uncompetitive	24.190	0.989
10	0.72	156.00	Uncompetitive	30.080	0.991
9	0.79	164.00	Uncompetitive	33.710	0.990
11	0.83	175.00	Uncompetititve	35.305	0.989
	For BChE inhibitory activity				
	BTC				
Inhibitors	K_m (mM)	V_{max} (mM min^{-1})	Type of inhibition	IC_{50} (μM)	R^2
Control	0.87	200.00	—	—	0.988
Donepezil	0.93	200.00	Competitive	40.360	0.987
13	3.33	200.00	Competitive	2.570	0.990
19	2.50	200.00	Competitive	6.890	0.990
12	1.79	200.00	Competitive	10.760	0.988
15	1.43	200.00	Competitive	15.130	0.989
14	1.28	200.00	Competitive	18.560	0.991
21	1.17	200.00	Competitive	21.930	0.995
22	0.51	141.00	Uncompetitive	27.250	0.987
8	0.54	150.00	Uncompetitive	29.780	0.991
6	0.59	146.00	Uncompetitive	31.720	0.992
23	0.66	160.00	Uncompetitive	36.410	0.993
7	0.77	185.00	Uncompetititve	38.920	0.987

2.560 ± 0.009 μM. The inhibition types of compounds **2** and **25** were assessed using Lineweaver–Burk plots with varying starch concentrations. Both compounds increased K_m while V_{max} (265.00 mM min^{-1}) remained unchanged, indicating competitive inhibition, in which the inhibitors compete with the substrate for the active site. Compound **2** showed the highest affinity (K_m = 1.25 mg mL^{-1}) among competitive inhibitors. In contrast, compounds **3**, **17**, and **18** decreased both K_m and V_{max}, consistent with uncompetitive inhibition, where the inhibitor binds only to the enzyme–substrate complex. Among these, compound **3** showed the strongest binding (K_m = 0.44 mg mL^{-1}; V_{max} = 215.00 mM min^{-1}) (Table 2 and Fig. 9A and B).

Kinetic studies on AChE and BChE enzymes

The synthesized derivatives were evaluated for AChE inhibitory activity by plotting the percentage relative activity against inhibitor concentration. Derivative **13** demonstrated the most potent inhibition, with an IC_{50} of 0.36 ± 0.01 μM. The compounds more active than donepezil ranked in potency as follows: **13** > **19** > **12** > **15** > **14** > **21** > **22** > **8** > **6** > **23** > **7** > **10** > **9** > **11** > donepezil (Tables 1 and 3).

The inhibition types of compounds **6–15**, **19**, **21–23**, and donepezil were determined using Lineweaver–Burk plots at varying ATC concentrations. Compounds **8**, **13**, **19**, **12**, **15**, **14**, **21**, and **22** increased K_m, while V_{max} (190.00 mM min^{-1}) remained unaffected, indicating competitive inhibition. Compound **13** displayed the highest affinity (K_m = 2.43 mM) (Fig. 10A). In contrast, compounds **6**, **23**, **7**, **10**, **9**, and **11** showed decreases in both Km and Vmax, suggesting uncompetitive inhibition, in which the inhibitor binds only to the enzyme–substrate complex. Compound **6** showed the strongest interaction among these (K_m = 0.56 mg mL^{-1}; V_{max} = 116.00 mM min^{-1}) (Fig. 10B).

In vitro BChE inhibition studies and kinetic results

All newly synthesized compounds were evaluated for BChE inhibitory activity by plotting the percentage relative activity against inhibitor concentration. Compound **13** showed the

strongest inhibition, with an IC_{50} of 2.57 ± 0.01 μM. The compounds more active than donepezil ranked in potency as follows: **13** > **19** > **12** > **15** > **14** > **21** > **22** > **8** > **6** > **23** > **7** > donepezil (Tables 1 and 3).

The inhibition types of compounds **13**, **19**, **12**, **15**, **14**, **21**, **22**, **8**, **6**, **23**, **7**, and donepezil were determined using Lineweaver–Burk plots with varying BTC concentrations. Compounds **13**, **19**, **12**, **15**, **14**, and **21** increased K_m while V_{max} (200.00 mM min^{-1}) remained unchanged, indicating competitive inhibition. Among these, compound **13** exhibited the highest affinity (K_m = 3.33 mM) (Fig. 11A). In contrast, compounds **22**, **8**, **6**, **23**, and **7** decreased both K_m and V_{max}, suggesting uncompetitive inhibition, where the inhibitor binds only to the enzyme–substrate complex. Out of these, derivative **22** presented the strongest interaction (K_m = 0.51 mg mL; V_{max} = 141.00 mM min^{-1}) (Fig. 11B).

Molecular docking studies analysis

Molecular docking was implemented on all alkyl and aryl piperate derivatives as well as on control acarbose with four

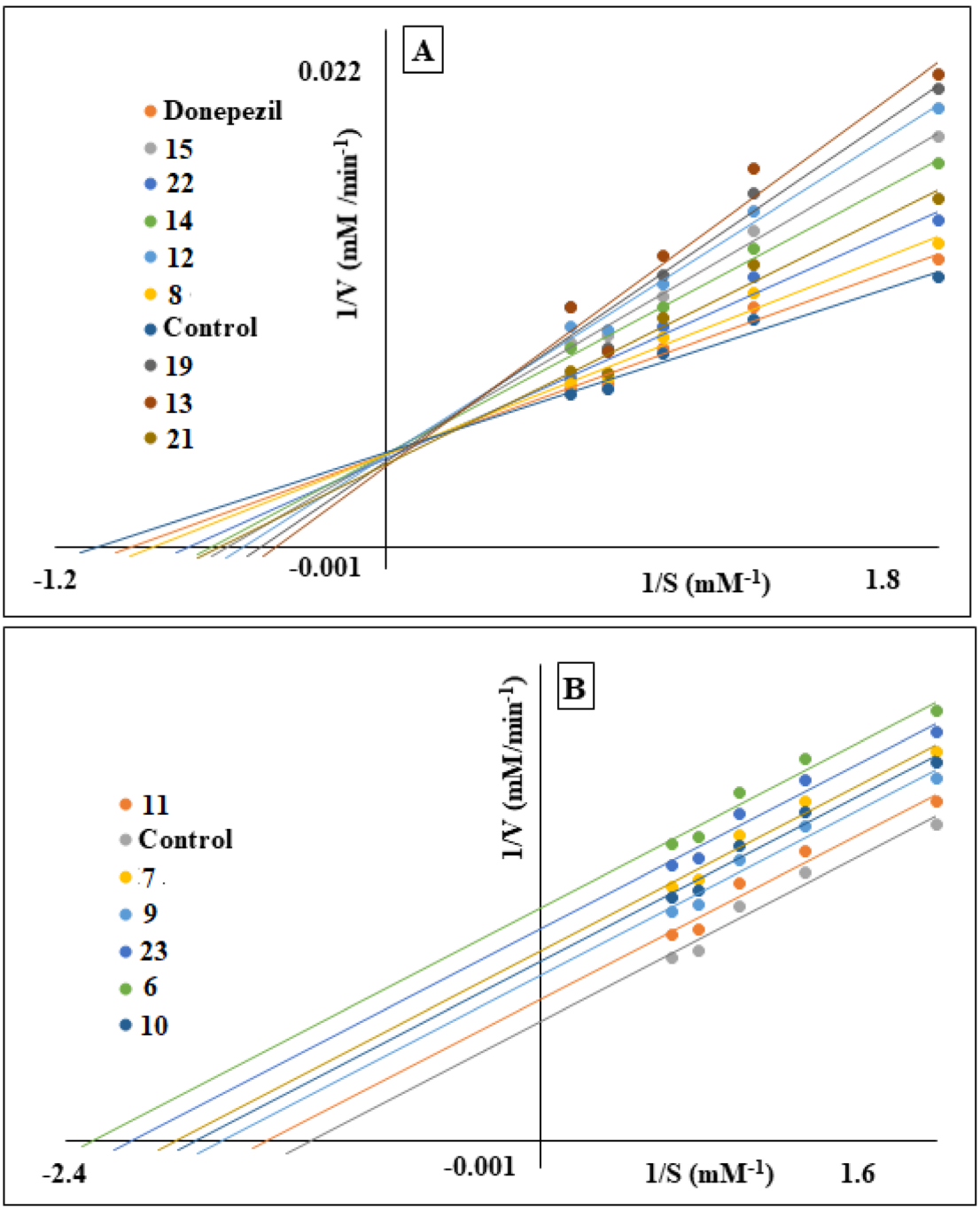

Fig. 10 Lineweaver–Burk plots of (A) donepezil and compounds **8**, **12**, **13**, **14**, **15**, **19**, **21**, and **22** showing competitive inhibition; (B) compounds **6**, **7**, **9**–**11**, and **23** showing uncompetitive inhibition against AChE.

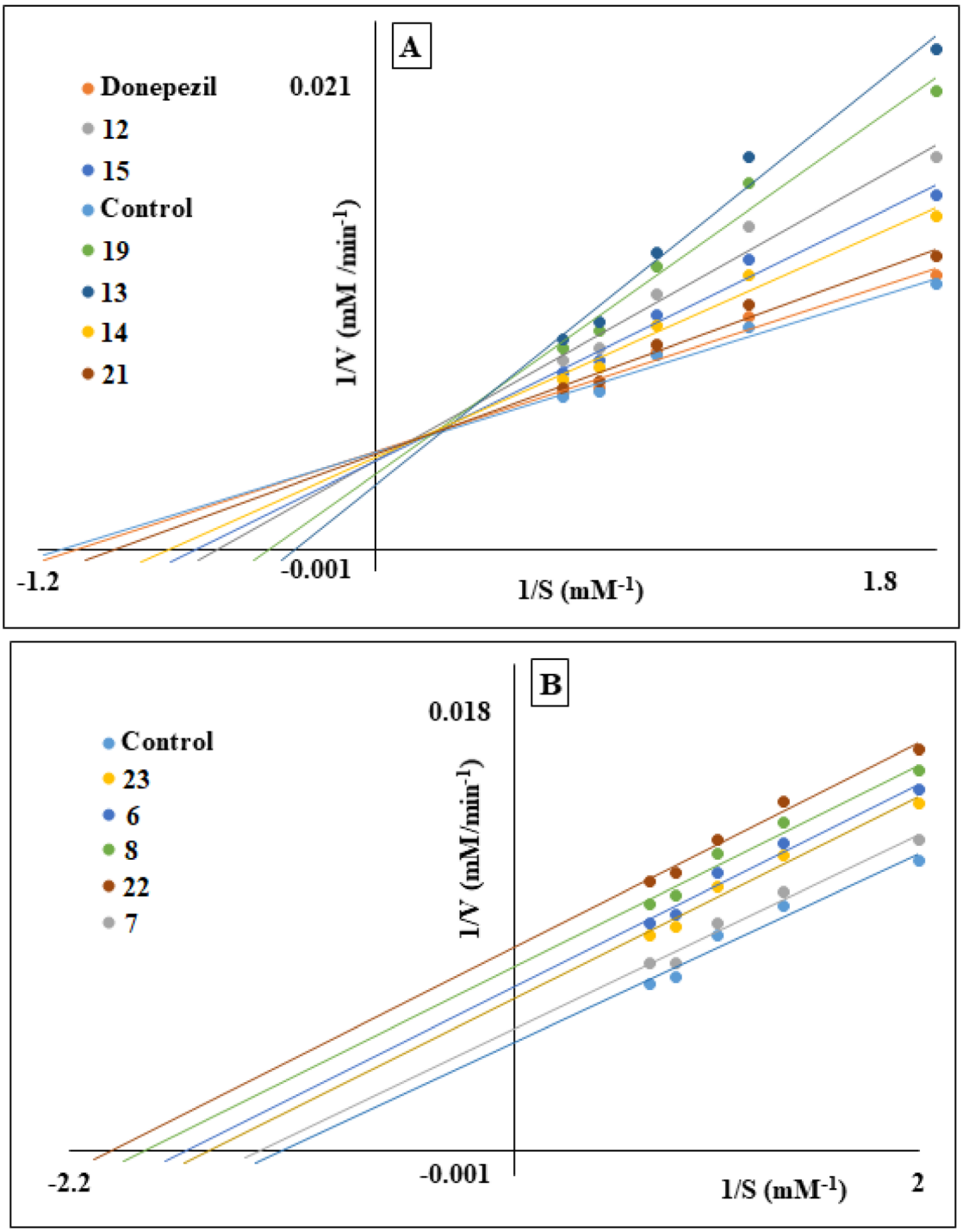

Fig. 11 Lineweaver–Burk plots of (A) donepezil and compounds **12**–**15**, **19**, and **21**, showing competitive inhibition; (B) compounds **6**–**8**, **22**, and **23** showing uncompetitive inhibition against BChE.

target proteins using their crystal structures, *i.e.*, α-amylase (PDB ID 1B2Y), α-glucosidase (PDB ID 3WY1), AChE (PDB ID 7E3H), and BChE (PDB ID 5DYW). The docking scores, residues participating in hydrogen bonding, and the corresponding bond distances are summarized in Tables S1–S4, alongside the IC_{50} values of the proteins of interest.

Molecular interactions of derivatives with α-amylase enzyme

The control, acarbose, formed multiple hydrogen-bond interactions with the active-site residues of α-amylase. Residues GLN63, THR163, and ARG195 formed interactions with atoms of the acarbose ring at distances of 3.00, 2.67, and 2.86 Å, respectively, while the top-ranked pose yielded a docking score of −9.087.

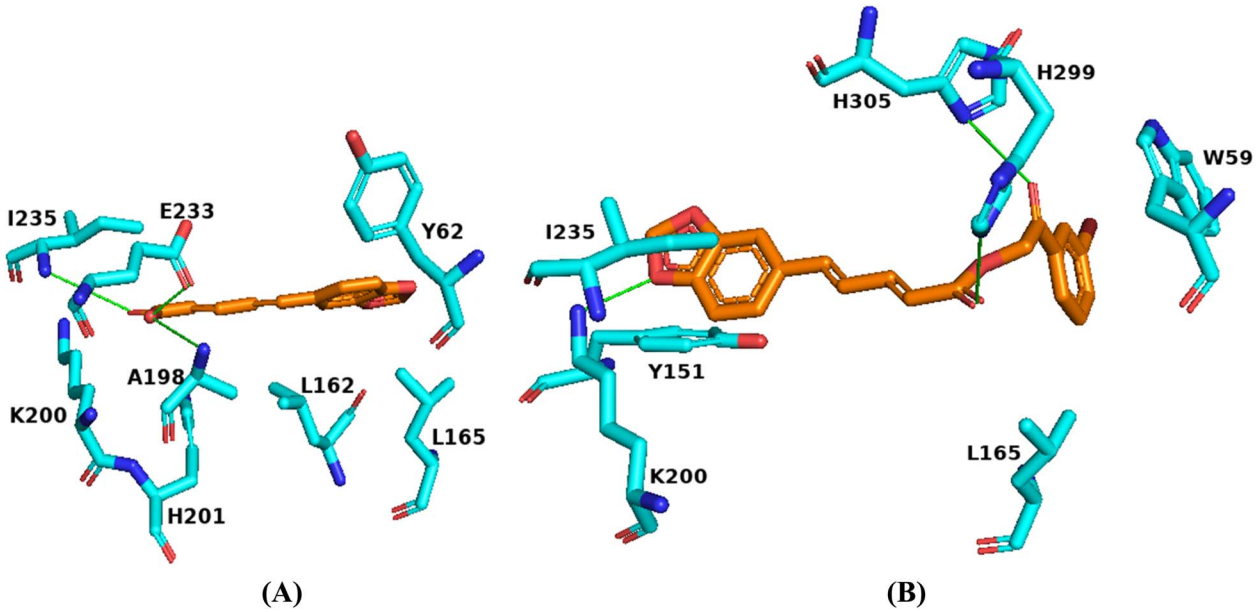

Fig. 12 Molecular interactions of compound 2 (A) and compound 23 (B) with the active pocket of α-amylase.

Derivatives **2**, **3**, **6**, **17**, **18**, **23**, and **25** with the lowest IC_{50s} showed the top-ranked poses, with docking scores of −4.8, −5.8, −6.7, −6.1, −6.9, −6.9, and −6.8, respectively. An in-depth interaction analysis revealed that the aforementioned compounds formed hydrogen bonds with residue LYS200, while hydrophobic interactions were observed with residues TRP58, TRP59, TYR62, TYR151, LEU165, LYS200, and ILE235 of α-amylase. The highest number of hydrogen bonds was observed for compounds **2** and **23**, which involved amino acids ALA198, GLU233, ILE235, and LYS200, HIS299, and HIS305, respectively. The docking scores recorded for all derivatives ranged from −5.9 to −7.02 (Fig. 12).

Among the α-amylase residues, GLN63, LYS200, and HIS299 were most frequently involved in hydrogen bonding with the alkyl and aryl piperate derivatives, whereas TRP59, TYR62, TYR151, and ILE235 predominantly contributed to hydrophobic interactions. These residues may thus play a critical role in stabilizing the α-amylase binding pocket.

Molecular interactions of derivatives with α-glucosidase enzyme

The standard inhibitor acarbose exhibited multiple hydrogen bond interactions with the active site residues of α-glucosidase, including ASP62, HIS105, ASP202, THR203, GLY228, ALA229, ASN301, ASN331, ASP333, TYR389, and ARG400, at distances of 3.02, 3.12, 2.22, 2.91, 1.87, 2.94, 3.07, 2.49, 3.55, 2.73, and 2.50 Å, respectively. The top-ranked pose yielded a docking score of −9.549.

Most potent derivatives **2**, **3**, **6**, **17**, **18**, **23**, and **25** with the lowest IC_{50} values, established the top-ranked pose and docking scores of −6.15, −7.92, −7.47, −8.516, −8.54, and −7.49, respectively. Detailed interaction analysis revealed that derivatives **2** formed hydrogen bonds with residues THR226, LEU227, GLY228, ALA229, HIS332, and ARG400 at distances of 3.07, 2.62, 2.09, 2.75, and 3.22 Å, respectively.

Compounds **6** and **17** formed hydrogen bond interactions with the residue GLN170, and compound 18 formed a hydrogen bond with THR226, all at distances of 3.13, 3.26, and 2.02 Å, respectively. Derivative **23** furnished hydrogen bond connections with residues ALA229, GLU271, HIS332, ARG400, and ARG404, while compound **25** presented hydrogen bonding with THR226, ALA229, and ARG400 at the bond distances of 2.43, 3.70, 2.19, 2.38, 3.06, 3.31, 3.07, and 2.16 Å, respectively. The highest number of hydrogen bonds was observed with compound **2**, which formed hydrogen bonds with THR226, LEU227, GLY228, ALA229, HIS332, and ARG400, respectively (Fig. 13). The docking scores recorded for all derivatives ranged between −6.15 and −7.49.

In α-glucosidase, GLN170, THR226, ALA229, and ARG400 were most frequently involved in hydrogen bonding with the

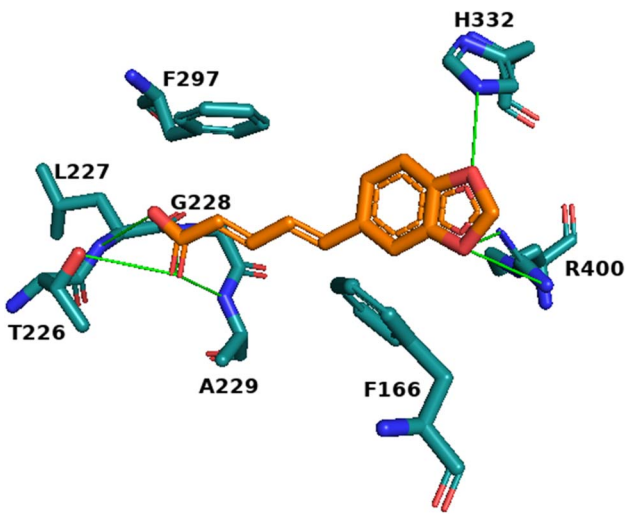

Fig. 13 Molecular interactions of compound 2 with the active pocket of α-glucosidase.

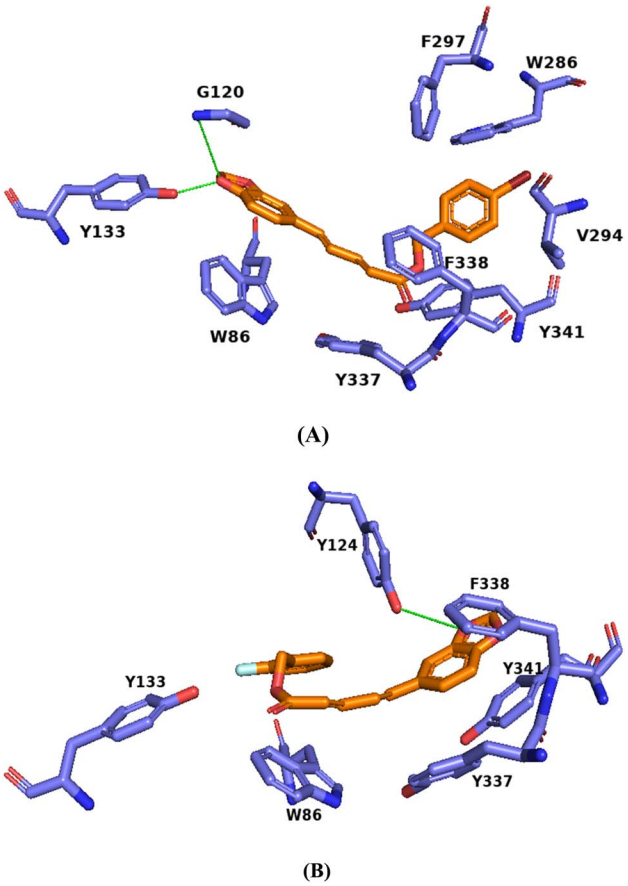

Fig. 14 Molecular interactions of compounds **6** (A) and **13** (B) with the active pocket of AChE.

derivatives, whereas TYR65, ILE146, PHE166, THR226, ALA229, PHE297, ASP333, TYR389, and ARG400 contributed to hydrophobic interactions. These residues can therefore be considered crucial for stabilizing the α-glucosidase binding pocket.

Molecular interactions of derivatives with AChE

In the case of alkyl and aryl piperate derivatives, the AChE residues most frequently forming hydrogen bonds are TYR133, PHE295, and ARG296, whereas TRP86, TRP286, TYR337, PHE338, and TYR341 primarily contribute through hydrophobic interactions. Collectively, these residues play a key role in stabilizing the AChE binding pocket.

The reference compound, donepezil, exhibited multiple hydrogen-bond interactions with AChE active-site residues, including TYR124 at 2.65 Å, as well as hydrophobic contacts involving TRP86, TRP286, VAL294, TYR337, PHE338, and TYR341. The top-ranked binding pose yielded a docking score of −8.70.

Compounds **6**, **8**, **12–15**, **19**, and **21–23** have the lowest IC_{50} s and show the top-ranked poses, with docking scores of −7.84, −7.56, −7.64, −7.78, −6.88, −7.14, −8.15, −8.66, −7.82, and −7.98, respectively. Molecular interaction analysis revealed that derivative **6** formed hydrogen bonds with AChE residues GLY120 (3.48 Å) and TYR133 (1.76 Å), along with hydrophobic interactions involving TRP86, TRP286, VAL294, PHE297, TYR337, PHE338, and TYR341. In contrast, compound **13** established a hydrogen bond with TYR124 at a distance of 3.01 Å (Fig. 14). In addition, derivatives **8**, **12**, **14**, **15**, **19**, **21**, **22**, and **23** present hydrogen bonding with PHE295 and ARG296, respectively. The docking scores for all derivatives ranged between −6.88 and −7.98.

Molecular interactions of derivatives with BChE

For the alkyl and aryl piperate derivatives, the BChE residues most frequently forming hydrogen bonds were TRP82, SER198, GLY117, and TRP430, whereas TRP82, TRP231, LEU286, VAL288, and PHE329 predominantly contributed through hydrophobic interactions. These residues are therefore considered critical for stabilizing the enzyme's binding pocket.

The reference donepezil formed hydrogen bonds with BChE residues THR120 (1.83 Å) and SER198 (2.36 Å), as well as hydrophobic interactions with TRP82, PHE329, TYR332, and TYR440. The top-ranked pose achieved a docking score of −8.21.

Compounds **8**, **12**, **13**, **14**, **15**, **19**, **21**, and **22** exhibited the lowest IC_{50} values, corresponding to top-ranked docking poses with scores of −7.26, −6.86, −7.05, −6.77, −7.17, −7.56, −7.62, and −7.45, respectively. Detailed interaction analysis showed that compound **21** did not form any hydrogen bonds, whereas compounds **8**, **12–15**, **19**, and **22** established hydrogen bonds with residues ASP70, GLN71, SER72, TRP82, GLY116, GLY117, SER198, ALA199, and TRP430, in addition to hydrophobic contacts with ASP70, TRP82, GLN119, THR120, TRP231, ALA277, LEU286, VAL288, PHE329, TYR332, and PHE398. Derivatives **8** and **22** displayed the highest number of hydrogen bonds (Fig. 15). Overall, the docking scores of these compounds ranged from −7.26 to −7.45.

Molecular dynamic simulation studies

Although molecular docking results have identified the best possible binding modes for the defined protein-ligand systems α-amylase_compound **2**, α-glucosidase_compound **2**, AChE_-compound **13**, and BChE_compound **22**, the smallest discrepancies can be evaluated by simulating molecular dynamics, including the details of atoms within the solvent system. Acarbose, for α-amylase and α-glucosidase, while donepezil for AChE and BChE, were selected as the reference compounds, respectively.

Molecular system stability can be inferred from Root Mean Squared Deviation (RMSD) values; the metric quantifies the average distance between atoms in a specific structure at different points in time relative to the reference structure. A system attaining lower deviations suggests the minimum structural change relative to the initial conformational state over the given simulation time period for each complex. In α-amylase_-compound **2**, the RMSD value of a backbone atom of protein about its initial state increased to 0.145 nm for the first 5 ns and maximally reached of 0.196 nm at 90.8 ns in the trajectory, a slight fluctuation of 0.21 nm at 28–32 ns, compared to reference structure was observed; overall a stable state of conformation was

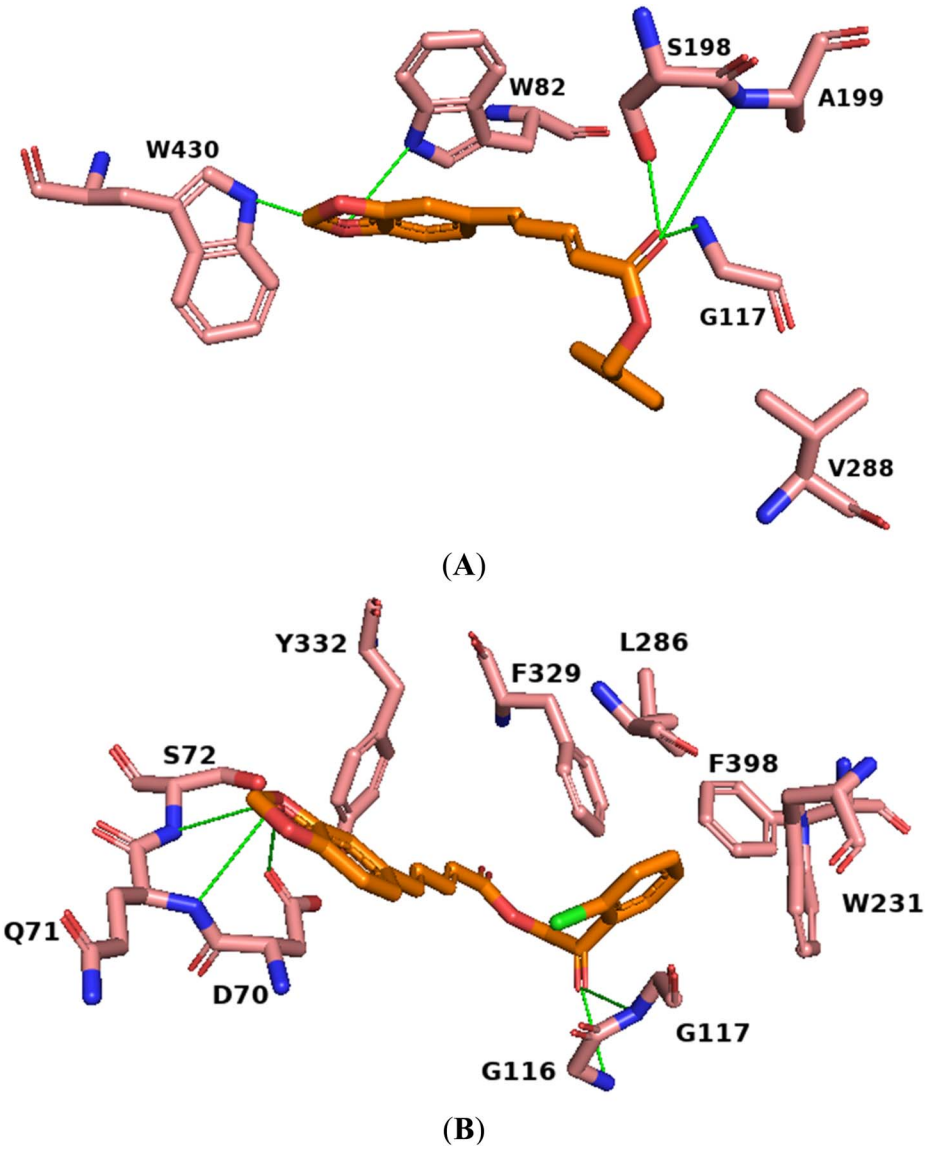

Fig. 15 Molecular interactions of compounds **8** (A) and **22** (B) with the active pocket of BChE.

maintained during the 100 ns simulation run (Fig. 16, top left panel). For α-glucosidase_compound **2**, initially the RMSD value of a protein's backbone atom increased to 0.15 nm for the first 5 ns, reaching 0.24 nm at 95 ns in the trajectory, and showed higher fluctuations for 40 ns with RMSD rising to 0.251–0.29 nm compared to the α-glucosidase_acarbose, indicating a moderate stability in conformation (Fig. 16, top right panel). The BChE_-compound **22** had shown slightly higher fluctuations with an RMSD value range of 0.23 nm, whereas initial peaks of higher fluctuation in complex AChE_compound **22** around 20–40 ns with an RMSD value of 0.22 nm were observed. Overall, the compounds formed stable complexes with the respective proteins relative to the reference structure during the simulation period, reflecting varying degrees of flexibility in the conformation with some magnitude differences. To further quantify the conformational flexibility in certain regions of the molecular systems, the RMSF metric has been assessed.

The RMSF measures the deviation of individual residues from their average positions over the simulation time period. Overall, the RMSF profile of each studied molecular system indicates structural stability; however, regions that exhibit sharp peaks of higher fluctuations, particularly the loop segment, are expected to play a vital role in the protein's conformational adaptability and are important for potential interactions with the respective compounds. The distinct peaks of higher fluctuation in α-amylase_compound **2** are located at residues 150, 240, 350, and 360, whereas in α-glucosidase, higher flexibility was observed at residues 245 and 248. For BChE_compound **22**, the fluctuation was higher near residue 340, and in AChE_compound **13**, a higher fluctuation peak was observed at position 500, relatively to the respective reference structures.

The compactness of the overall molecular structure was determined by radius of gyration (RoG) at different time points. For compound **2**, α-amylase maintained stability and structural

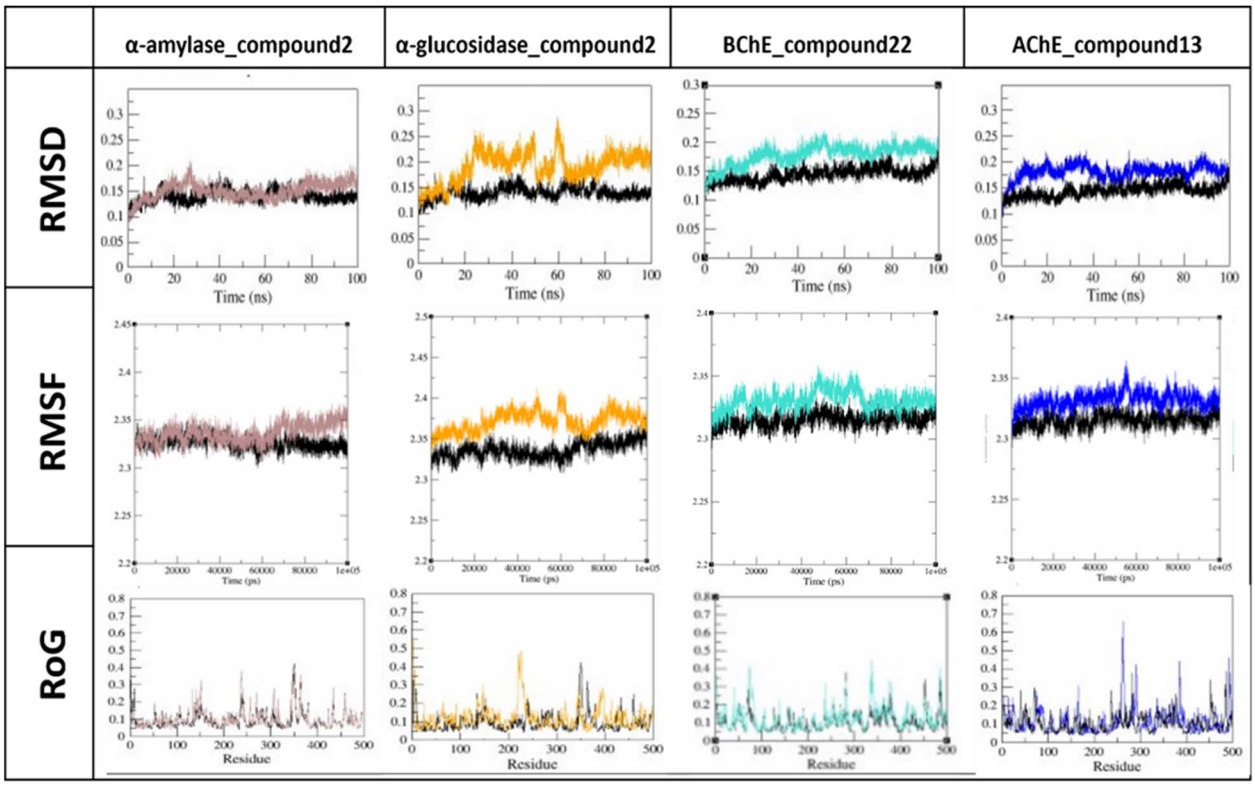

Fig. 16 The root means square deviation (RMSD), root mean square fluctuation (RMSF), and radius of gyration (RoG) plots of the protein complexes, α-amylase_compound **2** (brown color) and α-glucosidase_compound **2** (orange color), BChE_compound **22** (turquoise) and AChE_compound **13** (blue color) relative to their reference structure (black color) during the 100 ns trajectory of MD simulation, respectively.

compactness, with RoG values ranging from 2.35 nm; in contrast, certain regions around 30 ns in α-glucosidase exhibit moderate structural expansion, with RoG values exceeding 2.4 nm. While the complex BChE_compound **22** had shown no significant fluctuations and maintained its structural compactness with RoG value ranges 2.357 nm, the higher fluctuation of AChE_compound **13** at 260 residue number with RoG value of 2.33 nm was observed, compared to the reference structure throughout the 100 ns simulation run.

Antioxidant activity assay

Synthesized derivatives were also evaluated for antioxidant potential using CUPRAC, FRAP, and DPPH assays. The CUPRAC method measures antioxidant capacity by measuring the absorbance of the Cu(I)-neocuproine (Nc) complex formed when antioxidants reduce Cu(II)-Nc, with a maximum absorbance at 450 nm.[30] In the FRAP assay, antioxidants reduce Fe(III) to Fe(II), forming a TPTZ-Fe^{2+} complex measured at 593 nm. Absorbance values were converted to antioxidant capacity as μM $FeSO_4 \cdot 7H_2O$ equivalents using a calibration curve. Results are shown in Table 1. Compound **20** exhibited the strongest activity in both assays, with 126.083 ± 0.125 μM $FeSO_4 \cdot 7H_2O$ per mg (FRAP) and 8.579 ± 0.006 mM Trolox per mg (CUPRAC). The CUPRAC and FRAP results of other derivatives were within the range of 5.928–7.860 mM Trolox per mg compound, and 80.667–116.081 μM $FeSO_4 \cdot 7H_2O$ g^{-1} compound, respectively (Table 1). The DPPH assay measures antioxidant activity by the decrease in purple color of the DPPH radical at 517 nm upon reaction with an antioxidant. Results are reported as SC_{50} (μM), the concentration required to scavenge 50% of the radicals, determined from absorbance *vs.* concentration plots. Compound **20** was the best compared to the other synthesized derivatives, because it has the lowest SC_{50} value (95.280 ± 0.044 μM) (Table 1).

Pharmacokinetic, drug-likeness, and ADME studies

A detailed pharmacokinetics, drug-likeness, and ADME (absorption, distribution, metabolism, and excretion) assessment (Table 4) of all analogs and standard inhibitors (acarbose, donepezil chloride) was predicted using the SwissADME and PreADME online servers. Luckily, all synthetic analogs met Lipinski's Rule of Five and had no violations, indicating favorable physicochemical profiles. It also implies strong potential for all analogs in terms of oral bioavailability and as drug-like candidates. Relevant to add that the standard inhibitor acarbose showed three breaches of the Lipinski Rule of Five. The Caco-2 cell permeability data indicated that the higher-polarity analogs 2, 3, and 25 were low-permeable. In contrast, the rest of the analogs were moderate to good, with a range of 30–54 × 10^{-6} cm s^{-1}, representing good intestinal absorption. The predicted HIA (human intestinal absorption) values in the 90 s also showed that all analogs have strong potential for oral absorption. Besides, the BBB (blood–brain barrier) permeability

Table 4 Drug-likeness/ADME prediction of the most potent compounds **2–25**, and the standards acarbose and donepezil chloride[a]

Drug-likeness/ADME									
Comp.	Lipinski's rule of five	Caco2	HIA	BBB	Water solubility	Lipophilicity (XLOGP3)	Skin permeability	Bioavailability score (F)	Synthetic accessibility
Acarbose	No; 3 violations: MW > 500, NorO > 10, NHorOH > 5	1.94459	92.870605	0.306239	Highly soluble	−8.82	−16.50	0.17	7.25
Donepezil chloride	Yes, 0 violation	56.7456	99.024038	0.172463	Moderately soluble	4.79	−5.42	0.55	3.53
2	Yes, 0 violation	7.57786	97.143296	0.0125961	Soluble	3.23	−5.34	0.85	2.74
3	Yes, 0 violation	10.6706	97.365216	0.0163317	Soluble	3.35	−5.49	0.55	2.96
4	Yes, 0 violation	51.5253	97.948705	0.163868	Moderately soluble	5.35	−4.26	0.55	3.29
5	Yes, 0 violation	49.5354	97.924709	0.0538538	Moderately soluble	4.67	−4.65	0.55	3.24
6	Yes, 0 violation	52.199	97.720120	0.129504	Moderately soluble	4.84	−5.23	0.55	3.25
7	Yes, 0 violation	52.1789	97.720120	0.128222	Moderately soluble	4.84	−5.23	0.55	3.33
8	Yes, 0 violation	53.0137	97.578154	0.11859	Moderately soluble	4.78	−5.00	0.55	3.22
9	Yes, 0 violation	54.3628	97.792373	0.260966	Moderately soluble	5.41	−4.76	0.55	3.28
10	Yes, 0 violation	54.3821	97.792373	0.272641	Moderately soluble	5.41	−4.76	0.55	3.32
11	Yes, 0 violation	54.2164	97.792373	0.28198	Moderately soluble	5.41	−4.76	0.55	3.31
12	Yes, 0 violation	53.498	97.580831	0.147953	Moderately soluble	4.88	−5.04	0.55	3.29
13	Yes, 0 violation	52.5179	97.538737	0.0731802	Moderately soluble	4.25	−5.27	0.55	3.21
14	Yes, 0 violation	43.4642	97.520794	0.162157	Moderately soluble	5.04	−5.02	0.55	3.35
15	Yes, 0 violation	43.9142	97.520794	0.165651	Moderately soluble	5.04	−5.02	0.55	3.37
16	Yes, 0 violation	51.6013	97.531706	0.224138	Moderately soluble	5.28	−4.69	0.55	3.49
17	Yes, 0 violation	51.5353	97.568347	0.0491547	Moderately soluble	4.12	−5.44	0.55	3.47
18	Yes, 0 violation	41.1654	98.608102	0.0648324	Moderately soluble	4.04	−5.67	0.55	3.47
19	Yes, 0 violation	44.4873	98.598133	0.049763	Moderately soluble	4.14	−5.71	0.55	3.48
20	Yes, 0 violation	35.8406	97.887328	0.0430259	Moderately soluble	4.43	−5.29	0.55	3.36
21	Yes, 0 violation	30.9868	97.857063	0.0735752	Moderately soluble	4.95	−5.25	0.55	3.35
22	Yes, 0 violation	38.0499	97.508087	0.0499529	Moderately soluble	4.70	−5.22	0.55	3.29
23	Yes, 0 violation	36.8603	97.407121	0.048257	Moderately soluble	4.76	−5.45	0.55	3.35
24	Yes, 0 violation	36.7139	98.170765	0.0485777	Moderately soluble	4.72	−5.77	0.55	3.37
25	Yes, 0 violation	14.4809	96.404562	0.375647	Moderately soluble	3.90	−5.86	0.55	3.38

[a] The recommended ranges for Caco2: <25 poor, >50 great, HIA: >80% is high <25% is poor, Blood–Brain Barrier (BBB) = logBB > 0.3 readily crosses BBB (CNS active), < −1 poorly penetrates BBB, lipophilicity (XLOGP3) = −0.7 – +6.0, and skin_permeability = −8.0 – −1.0; bioavailability score (F): ≥ 0.55 is considered ideal and absorbed very well by the body.

data indicated that compound 25 exhibited a higher predicted BBB permeability (>0.3) and could penetrate the CNS (central nervous system). But the remaining analogs with lower BBB permeability could be beneficial in cases where CNS exposure is not required. On the whole, the results of this study indicate promising prospects of the piperate analogs as orally active candidates with favorable absorption profiles.

Moreover, compounds **2** and **3** showed good water solubility, and the remaining compounds exhibited moderately soluble predicted profiles, which justify their good potential for absorption and formulation. The XLOGP3 value was predicted to fall within a reasonable range (3.2 to 5.4), indicating a good balance of hydrophilicity and lipophilicity to enable oral absorption. The skin permeability $\log K_p$ values range from −4.26 to −5.86, indicating generally low transdermal permeation, consistent with the intended systemic use. Furthermore, the uniform bioavailability score of 0.55 across all compounds, including donepezil chloride, implied a reasonable probability of achieving adequate oral bioavailability, reinforcing their potential as orally active therapeutic candidates. All compounds had a predicted synthetic accessibility score between 2.74 and 3.49, indicating their relative ease of synthesis and potential for further development.

Conclusion

A library of twenty-four (24) alkyl and aryl piperate derivatives was synthesized, structurally characterized, and assessed for their multitarget potential against validated drug targets of DM and AD. To date, 21 derivatives are new, while 3 were already reported structurally. Several compounds were identified as being much more potent against α-glucosidase, α-amylase, AChE, and BChE, highlighting their potential as lead candidates for the development of novel antidiabetic and anti-Alzheimer's agents. To support the *in vitro* inhibitory results, kinetic studies were conducted to elucidate the inhibition mechanism for all four enzymes, while *in silico* studies highlighted the key interactions between the inhibitors and the active-site residues of each enzyme. SAR provides a clear direction for future optimization, focusing on minimal, well-placed substituents to maximize inhibitory efficiency. All compounds also displayed reasonable antioxidant potential, as determined by the CUPRAC, FRAP, and DPPH methods. Pharmacokinetics and ADME analysis suggest that the compounds have optimal physicochemical properties and favorable ADME (absorption, distribution, metabolism, excretion) profiles, making them potential drug candidates. The identified compounds have multitarget inhibitory potential against key enzymes linked to diabetes and Alzheimer's, suggesting they could make significant contributions in subsequent stages of drug development.

Consent for publication

All authors have read and approved the final version of the manuscript.

Author contributions

Asif Ahmad: synthesis, data acquisition, characterization of target compounds, and original manuscript writing. Uzma Salar: design, methodology, characterization of target compounds, formal analysis, supervision, review, editing, and authentication of the final draft of the manuscript. Farzana Shaheen and Khalid Mohammed Khan: overall supervision of the project, including formal analysis, review, editing, funding acquisition, and authentication of the final manuscript draft. Musa Özil and Nimet Baltaş: bioassay methodology, performed *in vitro* bioactivities and kinetics studies of all compounds, formal analysis, review, and editing of the manuscript. Aaqib Ullah: data acquisition, characterization of target compounds, and original manuscript writing. Maria Nasim and Zaheer Ul Haq: performed *in silico* studies of the compounds, reviewed, and edited the manuscript.

Conflicts of interest

The authors declare no conflicts of interest, financial or otherwise. No writing assistance was utilized in the production of this manuscript.

Data availability

All associated data is provided in this submission.

Supplementary information (SI) is available. See DOI: https://doi.org/10.1039/d6ra00843g.

Acknowledgements

Asif Ahmad acknowledges the Sindh Higher Education Commission, Pakistan, for sanctioning the Indigenous Scholarship (FY2022-23).

References

1 F. Saleem, F. Naz and K. M. Khan, Patent analysis of novel therapeutic approaches for treating Alzheimer's disease, 2018-2023, *Pharm. Patent Anal.*, 2023, **12**, 91–94.
2 I. Grundke-Iqbal, K. Iqbal, Y. C. Tung, M. Quinlan, H. M. Wisniewski and L. I. Binder, Abnormal phosphorylation of the microtubule-associated protein tau (tau) in Alzheimer's cytoskeletal pathology, *Alzheimer's Dis. Assoc. Disord.*, 1987, **1**, 202.
3 A. Castro and A. Martinez, Targeting beta-amyloid pathogenesis through acetylcholinesterase inhibitors, *Curr. Pharm. Des.*, 2006, **12**, 4377–4387.
4 A. Gella and N. Durany, Oxidative stress in Alzheimer's disease, *Cell Adhes. Migr.*, 2009, **3**, 88–93.
5 J. T. Coyle and P. Puttfarcken, Oxidative stress, glutamate, and neurodegenerative disorders, *Science*, 1993, **262**, 689–695.
6 M. A. Ansari and S. W. Scheff, Oxidative stress in the progression of Alzheimer's disease in the frontal cortex, *J. Neuropathol. Exp. Neurol.*, 2010, **69**, 155–167.
7 Y. He, P. F. Yao, S. B. Chen, Z. H. Huang, S. L. Huang, J. H. Tan and Z. S. Huang, Synthesis and evaluation of 7,8-dehydrorutaecarpine derivatives as potential multifunctional agents for the treatment of Alzheimer's disease, *Eur. J. Med. Chem.*, 2013, **63**, 299–312.
8 Y. Chen, J. Sun, L. Fang, M. Liu, S. Peng, H. Liao and Y. Zhang, Tacrine-ferulic acid-nitric oxide (NO) donor trihybrids as potent multifunctional acetyl- and butyrylcholinesterase inhibitors, *J. Med. Chem.*, 2012, **55**, 4309–4321.

9 M. Mansha, M. Taha and N. Ullah, The design of fluoroquinolone-based cholinesterase inhibitors: synthesis, biological evaluation, and *in silico* docking studies, *Arab. J. Chem.*, 2021, **14**, 103211.

10 J. Joubert, G. B. Foka, B. P. Repsold, D. W. Oliver, E. Kapp and S. F. Malan, Synthesis and evaluation of 7-substituted coumarin derivatives as multimodal monoamine oxidase-B and cholinesterase inhibitors for the treatment of Alzheimer's disease, *Eur. J. Med. Chem.*, 2017, **125**, 853–864.

11 I. Tomassoli, L. Ismaili, M. Pudlo, C. de Los Ríos, E. Soriano, I. Colmena and B. Refouvelet, Synthesis, biological assessment, and molecular modeling of new dihydroquinoline-3-carboxamides and dihydroquinoline-3-carbohydrazide derivatives as cholinesterase inhibitors and Ca channel antagonists, *Eur. J. Med. Chem.*, 2011, **46**, 1–10.

12 B. Kumar, A. K. Mantha and V. Kumar, Recent developments on the structure-activity relationship studies of MAO inhibitors and their role in different neurological disorders, *RSC Adv.*, 2016, **6**, 42660–42683.

13 Q. H. Liu, J. J. Wu, F. Li, P. Cai, X. L. Yang, L. Y. Kong and X. B. Wang, Synthesis and pharmacological evaluation of multifunctional homoisoflavonoid derivatives as potent inhibitors of monoamine oxidase B and cholinesterase for the treatment of Alzheimer's disease, *MedChemComm*, 2017, **8**, 1459–1467.

14 M. Cisneros-Yupanqui, A. Lante, D. Mihaylova, A. I. Krastanov and C. Rizzi, The α-amylase and α-glucosidase inhibition capacity of grape pomace: a review, *Food Bioprocess Technol.*, 2023, **16**, 691–703.

15 D. Zelelew, M. Endale, Y. Melaku, T. Geremew, R. Eswaramoorthy, L. T. Tufa and J. Lee, Ultrasonic-assisted synthesis of heterocyclic curcumin analogs as antidiabetic, antibacterial, and antioxidant agents combined with *in vitro* and *in silico* studies, *Adv. Appl. Bioinform. Chem.*, 2023, 61–91.

16 I. Kabach, N. Bouchmaa, Z. Zouaoui, A. Ennoury, S. El Asri, A. Laabar and R. B. Mrid, Phytochemical profile and antioxidant capacity, α-amylase and α-glucosidase inhibitory activities of *Oxalis pes-caprae* extracts in alloxan-induced diabetic mice, *Biomed. Pharmacother.*, 2023, **160**, 114393.

17 F. T. Zahra, A. Saeed, A. Ahmed, H. Ismail, M. U. Ijaz and F. Albericio, Synthesis of amantadine clubbed *N*-aryl amino thiazoles as potent urease, α-amylase and α-glucosidase inhibitors: kinetic and molecular docking studies, *RSC Adv.*, 2023, **13**, 24988–25001.

18 H. Ullah, T. Batool, A. Nawaz, F. Rahim, F. Khan and A. Hussain, Synthesis, *in vitro* α-glucosidase and α-amylase inhibitory potentials and molecular docking study of benzimidazole bearing sulfonamide analogues, *Chem. Data Collect.*, 2023, **47**, 101070.

19 U. Salar, K. M. Khan, S. Chigurupati, S. Syed, S. Vijayabalan, A. Wadood, M. Riaz, M. Ghufran and S. Perveen, New hybrid scaffolds based on hydrazinyl thiazole substituted coumarin as novel leads of dual potential: *in vitro* α-amylase inhibitory and antioxidant (DPPH and ABTS radical scavenging) activities, *Med. Chem.*, 2019, **15**, 87–101.

20 O. Demirkiran, M. A. Mesaik, H. Beynek, A. Abbaskhan and M. I. Choudhary, Cellular reactive oxygen species inhibitory constituents of *Hypericum thasium* Griseb, *Phytochemistry*, 2009, **70**, 244–249.

21 M. Singh and O. Silakari, Design, synthesis and biological evaluation of novel 2-phenyl-1-benzopyran-4-one derivatives as potential polyfunctional anti-Alzheimer's agents, *RSC Adv.*, 2016, **6**, 108411–108422.

22 U. H. Park, H. S. Jeong, E. Y. Jo, T. Park, S. K. Yoon, E. J. Kim and S. J. Um, Piperine, a component of black pepper, inhibits adipogenesis by antagonizing PPARγ activity in 3T3-L1 cells, *J. Agric. Food Chem.*, 2012, **60**, 3853–3860.

23 C. Kharbanda, M. S. Alam, H. Hamid, K. Javed, S. Bano, Y. Ali and M. Q. Pasha, Novel piperine derivatives with antidiabetic effect as PPAR-γ agonists, *Chem. Biol. Drug Des.*, 2016, **88**, 354–362.

24 P. Chonpathompikunlert, J. Wattanathorn and S. Muchimapura, Piperine, the main alkaloid of Thai black pepper, protects against neurodegeneration and cognitive impairment in an animal model of cognitive deficit-like condition of Alzheimer's disease, *Food Chem. Toxicol.*, 2010, **48**, 798–802.

25 Z. Zarai, E. Boujelbene, N. B. Salem, Y. Gargouri and A. Sayari, Antioxidant and antimicrobial activities of various solvent extracts, piperine, and piperic acid from *Piper nigrum*, *LWT-Food Sci. Technol.*, 2013, **50**, 634–641.

26 A. Sivashanmugam and S. Velmathi, Bioactive component of black pepper-piperine: structure-activity relationship and its broad-spectrum activity-an overview, *Chem. Biol. Potent Nat. Prod. Synth. Compd.*, 2021, 43–92.

27 A. Yasir, S. Ishtiaq, M. Jahangir, M. Ajaib, U. Salar and K. M. Khan, Biology-oriented synthesis (BIOS) of piperine derivatives and their comparative analgesic and antiinflammatory activities, *Med. Chem.*, 2018, **14**, 269–280.

28 A. Sivashanmugam and S. Velmathi, Synthesis, *in vitro* and *in silico* antibacterial analysis of piperine and piperic ester analogues, *Chem. Biol. Drug Des.*, 2021, **98**, 19–29.

29 S. J. Souza Jr., P. S. E. Martins, D. S. H. Souza, R. F. Oliveira, F. S. Alves, E. O. Lima, L. V. Cordeiro, T. O. Emmely, B. F. Lira, G. B. Rocha, P. F. de Athayde-Filho and J. M. Barbosa-Filho, Synthesis, spectroscopic characterization, DFT calculations and preliminary antifungal activity of new piperine derivatives, *J. Braz. Chem. Soc.*, 2021, **32**, 490–502.

30 S. Hameed, K. M. Khan, U. Salar, M. Özil, N. Baltaş, F. Saleem, U. Qureshi, M. Taha and Z. Ul-Haq, Hydrazinyl thiazole-linked indenoquinoxaline hybrids: potential leads to treat hyperglycemia and oxidative stress; multistep synthesis, α-amylase, α-glucosidase inhibitory and antioxidant activities, *Int. J. Biol. Macromol.*, 2022, **221**, 1294–1312.

31 F. Saleem, K. M. Khan, N. Ullah, M. Özil, N. Baltaş, S. Hameed, U. Salar, A. Wadood, A. U. Rehman, M. Kumar, M. Taha and S. M. Haider, Bioevaluation of synthetic pyridones as dual inhibitors of α-amylase and α-glucosidase enzymes and potential antioxidants, *Arch. Pharm.*, 2023, **356**, e2200400.

32 H. Lineweaver and D. Burk, The determination of enzyme dissociation constant, *J. Am. Chem. Soc.*, 1934, **56**, 658–661.
33 P. S. Unnikrishnan, K. Suthindhiran and M. A. Jayasri, Alpha-amylase inhibition and antioxidant activity of marine green algae and their possible role in diabetes management, *Pharmacogn. Mag.*, 2015, **11**, 511–515.
34 G. L. Ellman, K. D. Courtney, V. Andres and R. M. Featherstone, A new and rapid colorimetric determination of acetylcholinesterase activity, *Biochem. Pharmacol.*, 1961, **7**, 88–95.
35 M. Maqbool, M. Solangi, K. M. Khan, M. Özil, N. Baltaş, U. Salar and M. Taha, Imidazole-thiadiazole hybrids: a multitarget *de novo* drug design approach, *in vitro* evaluation, ADME/T and *in silico* studies, *Arch. Pharm.*, 2024, **357**, e2400325.
36 S. Patodia, A. Bagaria and D. Chopra, Molecular dynamics simulation of proteins: a brief overview, *J. Phys. Chem. Biophys.*, 2014, **4**, 1.
37 M. J. Abraham, T. Murtola, R. Schulz, S. Páll, J. C. Smith, B. Hess and E. Lindahl, GROMACS: high performance molecular simulations through multi-level parallelism from laptops to supercomputers, *SoftwareX*, 2015, **1**, 19–25.
38 K. Lindorff-Larsen, S. Piana, K. Palmo, P. Maragakis, J. L. Klepeis, R. O. Dror and D. E. Shaw, Improved side-chain torsion potentials for the Amber ff99SB protein force field, *Proteins*, 2010, **78**, 1950–1958.
39 A. W. Sousa da Silva and W. F. Vranken, ACPYPE-Antechamber python parser interface, *BMC Res. Notes*, 2012, **5**, 1–8.
40 P. Mark and L. Nilsson, Structure and dynamics of the TIP3P, SPC and SPC/E water models at 298 K, *J. Phys. Chem. A*, 2001, **105**, 9954–9960.
41 M. Fernández-Pendás, B. Escribano, T. Radivojević and E. Akhmatskaya, Constant pressure hybrid Monte Carlo simulations in GROMACS, *J. Mol. Model.*, 2014, **20**, 1–10.
42 P. Turner, *XMGRACE, Version 5.1.19, Center for Coastal and Land-Margin Research*, Oregon Graduate Institute of Science and Technology, Beaverton, 2005.
43 M. Özil, G. Tacal, N. Baltaş and M. Emirik, Synthesis and molecular docking studies of novel triazole derivatives as antioxidant agents, *Lett. Org. Chem.*, 2020, **17**, 309–320.
44 A. Ahmad, U. Salar, M. Özil, N. Baltaş, S. S. Tariq, Z. Ul-Haq, K. M. Khan and F. Shaheen, Piperonal-derived (*E*)-2-(2-(benzo[*d*][1,3]dioxol-5-ylmethylene)hydrazineyl)-4-(aryl) thiazole derivatives as potential therapeutic leads for diabetes and Alzheimer's disease: *in vitro* and *in silico* evaluation against α-glucosidase, α-amylase, acetylcholinesterase and butyrylcholinesterase, *J. Mol. Struct.*, 2025, **1338**, 142306.
45 W. Brand-Williams, M. E. Cuvelier and C. Berset, Use of a free radical method to evaluate antioxidant activity, *LWT-Food Sci. Technol.*, 1995, **28**, 25–30.
46 S. K. Lee, I. H. Lee, H. J. Kim, *et al.*, PreADME: virtual screening for early ADME prediction, *Proc. Korea Genome Conf.*, 2002, 46–1.
47 A. Daina, O. Michielin and V. Zoete, SwissADME: a free web tool to evaluate pharmacokinetics, drug-likeness and medicinal chemistry friendliness of small molecules, *Sci. Rep.*, 2017, **7**, 42717.